Gigapixel microscopy using a flatbed scanner

Guoan Zheng,* Xiaoze Ou, and Changhuei Yang

Department of Electrical Engineering, California Institute of Technology, Pasadena, CA 91125, USA

*gazheng@caltech.edu

Abstract: Microscopy imaging systems with a very wide field-of-view (FOV) are highly sought in biomedical applications. In this paper, we report a wide FOV microscopy imaging system that uses a low-cost scanner and a closed-circuit-television (CCTV) lens. We show that such an imaging system is capable to capture a 10 mm * 7.5 mm FOV image with 0.77 micron resolution, resulting in 0.54 gigapixels (10^9 pixels) across the entire image (26400 pixels * 20400 pixels). The resolution and field curve of the proposed system were characterized by imaging a USAF resolution target and a hole-array target. A 1.6 gigapixel microscopy image (0.54 gigapixel with 3 colors) of a pathology slide was acquired by using such a system for application demonstration.

OCIS codes: (170.0110) Imaging systems; (170.4730) Optical pathology; (170.0180) Microscopy

References and links

1. M. Oheim, "Advances and challenges in high-throughput microscopy for live-cell subcellular imaging," Expert Opinion on Drug Discovery, 1-17 (2011).
2. A. VanderLugt, Optical signal processing (Wiley New York, 1992).
3. J. Gilbertson, J. Ho, L. Anthony, D. Jukic, Y. Yagi, and A. Parwani, "Primary histologic diagnosis using automated whole slide imaging: a validation study," BMC clinical pathology 6, 4 (2006).
4. http://www.dmetrix.net/techtutorial1.shtml.
5. G. Zheng, S. A. Lee, Y. Antebi, M. B. Elowitz, and C. Yang, "The ePetri dish, an on-chip cell imaging platform based on subpixel perspective sweeping microscopy (SPSM)," Proceedings of the National Academy of Sciences 108, 16889-16894 (2011).
6. W. Bishara, T. Su, A. Coskun, and A. Ozcan, "Lensfree on-chip microscopy over a wide field-of-view using pixel super-resolution," Optics Express 18, 11181-11191 (2010).
7. J. Wu, X. Cui, G. Zheng, Y. M. Wang, L. M. Lee, and C. Yang, "Wide field-of-view microscope based on holographic focus grid illumination," Optics letters 35, 2188-2190 (2010).
8. J. Wu, G. Zheng, Z. Li, and C. Yang, "Focal plane tuning in wide-field-of-view microscope with Talbot pattern illumination," Optics letters 36, 2179-2181 (2011).
9. J. Di, J. Zhao, H. Jiang, P. Zhang, Q. Fan, and W. Sun, "High resolution digital holographic microscopy with a wide field of view based on a synthetic aperture technique and use of linear CCD scanning," Applied optics 47, 5654-5659 (2008).
10. M. Lee, O. Yaglidere, and A. Ozcan, "Field-portable reflection and transmission microscopy based on lensless holography," Biomedical Optics Express 2, 2721-2730 (2011).
11. K. Fife, A. Gamal, and H. Wong, "A 3mpixel multi-aperture image sensor with 0.7 um pixels in 0.11 um cmos," in IEEE ISSCC Digest of Technical Papers, 2008), 48-49.
12. M. Ben-Ezra, "Large-Format Tile-Scan Camera," IEEE Computer Graphics and Applications, 49-61 (2011).
13. S. Wang and W. Heidrich, "The Design of an Inexpensive Very High Resolution Scan Camera System," Computer Graphics Forum 23, 441-450 (2004).
14. S. A. Lee, R. Leitao, G. Zheng, S. Yang, A. Rodriguez, and C. Yang, "Color Capable Sub-Pixel Resolving Optofluidic Microscope and Its Application to Blood Cell Imaging for Malaria Diagnosis," PloS one 6, e26127 (2011).
15. J. Mallon and P. F. Whelan, "Calibration and removal of lateral chromatic aberration in images," Pattern recognition letters 28, 125-135 (2007).
16. http://www.linhofstudio.com/products/cameras/anagramm_digital_reproduction/anagramm_digital_reproduction.html.
17. G. Zheng, C. Kolner, and C. Yang, "Microscopy refocusing and dark-field imaging by using a simple LED array," Optics letters 36, 3987-3989 (2011).

On the Technology Prospects and Investment Opportunities for Scalable Neuroscience

Thomas Dean[1,2,3] Biafra Ahanonu[3] Mainak Chowdhury[3]
Anjali Datta[3] Andre Esteva[3] Daniel Eth[3] Nobie Redmon[3]
Oleg Rumyantsev[3] Ysis Tarter[3]

1 Google Research, **2** Brown University, **3** Stanford University

Serb. Astron. J. № 1 (2013), 1 - 6

Original Scientific Paper

MASS EXTINCTION AND THE STRUCTURE OF THE MILKY WAY

M. D. Filipović[1], J. Horner[2,3], E. J. Crawford[1], N. F. H. Tothill[1]

[1] *University of Western Sydney, Locked Bag 1797, Penrith South DC, NSW 1797, Australia*
E–mail: *m.filipovic@uws.edu.au n.tothill@uws.edu.au e.crawford@uws.edu.au*

[2] *School of Physics, University of New South Wales, Sydney 2052, Australia*

[3] *Australian Centre for Astrobiology, University of New South Wales, Sydney 2052, Australia*
E–mail: *j.a.horner@unsw.edu.au*

(Received: August 2013; Accepted: September 2013)

SUMMARY: We use the most up to date Milky Way model and solar orbit data in order to test the hypothesis that the Sun's galactic spiral arm crossings cause mass extinction events on Earth. To do this, we created a new model of the Milky Way's spiral arms by combining a large quantity of data from several surveys. We then combined this model with a recently derived solution for the solar orbit to determine the timing of the Sun's historical passages through the Galaxy's spiral arms. Our new model was designed with a symmetrical appearance, with the major alteration being the addition of a spur at the far side of the Galaxy. A correlation was found between the times at which the Sun crosses the spiral arms and six known mass extinction events. Furthermore, we identify five additional historical mass extinction events that might be explained by the motion of the Sun around our Galaxy. These five additional significant drops in marine genera that we find include significant reductions in diversity at 415, 322, 300, 145 and 33 Myr ago. Our simulations indicate that the Sun has spent ∼60% of its time passing through our Galaxy's various spiral arms. Also, we briefly discuss and combine previous work on the Galactic Habitable Zone with the new Milky Way model.

Key words. Galaxy: structure – Physical data and processes: Astrobiology – Solar system: general – Galaxy: solar neighbourhood

1. INTRODUCTION

Mass extinctions have the effect of wiping the biological slate clean, freeing up ecological niches and thus producing explosions in biodiversity (e.g. McElwain and Punyasena 2007; Alroy 2008). In the past, several explanations have been proposed to resolve ancient mass extinctions, including vast outpourings of flood basalt (such as the Deccan and Siberian Traps; e.g. Wignall 2001), periods of global glaciation (Mayhew et al. 2008) and the impact of large asteroids and comets upon the Earth (e.g. Alvarez et al. 1980; Bottke et al. 2007). Of these, extreme geological and climate phenomena such as flood basalt outpouring and "snowball Earth" glaciations appear to be very rare and randomly-occurring events in the Earth's history. Overholt et al. (2009) investigate Earth's climate as a function of location in the Galaxy, however, no obvious correlation could be drawn. On the other hand, it is well established that the Earth has been continually pummelled by asteroidal and cometary impactors throughout its history, a process that will continue well into the fu-

A Roadmap to Interstellar Flight

Philip Lubin
Physics Dept, UC Santa Barbara
lubin@deepspace.ucsb.edu
submitted to JBIS April 2015
JBIS Vol. 69, pp. 40-72 Feb 2016
Current version 15–w7-4 (10/18/16)

Abstract – In the nearly 60 years of spaceflight we have accomplished wonderful feats of exploration that have shown the incredible spirit of the human drive to explore and understand our universe. Yet in those 60 years we have barely left our solar system with the Voyager 1 spacecraft launched in 1977 finally leaving the solar system after 37 years of flight at a speed of 17 km/s or less than 0.006% the speed of light. As remarkable as this, to reach even the nearest stars with our current propulsion technology will take 100 millennium. We have to radically rethink our strategy or give up our dreams of reaching the stars, or wait for technology that does not currently exist. While we all dream of human spaceflight to the stars in a way romanticized in books and movies, it is not within our power to do so, nor it is clear that this is the path we should choose. We posit a path forward, that while not simple, it is within our technological reach. We propose a roadmap to a program that will lead to sending relativistic probes to the nearest stars and will open up a vast array of possibilities of flight both within our solar system and far beyond. Spacecraft from gram level complete spacecraft on a wafer ("wafersats") that reach more than ¼ c and reach the nearest star in 20 years to spacecraft with masses more than 10^5 kg (100 tons) that can reach speeds of greater than 1000 km/s. These systems can be propelled to speeds currently unimaginable with existing propulsion technologies. To do so requires a fundamental change in our thinking of both propulsion and in many cases what a spacecraft is. In addition to larger spacecraft, some capable of transporting humans, we consider functional spacecraft on a wafer, including integrated optical communications, imaging systems, photon thrusters, power and sensors combined with directed energy propulsion. The costs can be amortized over a very large number of missions beyond relativistic spacecraft as such planetary defense, beamed energy for distant spacecraft, sending power back to Earth, stand-off composition analysis of solar system targets, long range laser communications, SETI searches and even terra forming. Exploring the nearest stars and exo-planets would be a profound voyage for humanity, one whose non-scientific implications would be enormous. It is time to begin this inevitable journey far beyond our home.

Generating Natural Language Inference Chains

Vladyslav Kolesnyk and **Tim Rocktäschel** and **Sebastian Riedel**
University College London
London, UK
vladyslav.kolesnyk.12@ucl.ac.uk, {t.rocktaschel,s.riedel}@cs.ucl.ac.uk

Abstract

The ability to reason with natural language is a fundamental prerequisite for many NLP tasks such as information extraction, machine translation and question answering. To quantify this ability, systems are commonly tested whether they can recognize textual entailment, *i.e.*, whether one sentence can be inferred from another one. However, in most NLP applications only single source sentences instead of sentence pairs are available. Hence, we propose a new task that measures how well a model can *generate* an entailed sentence from a source sentence. We take entailment-pairs of the Stanford Natural Language Inference corpus and train an LSTM with attention. On a manually annotated test set we found that 82% of generated sentences are correct, an improvement of 10.3% over an LSTM baseline. A qualitative analysis shows that this model is not only capable of shortening input sentences, but also inferring new statements via paraphrasing and phrase entailment. We then apply this model recursively to input-output pairs, thereby generating natural language inference chains that can be used to automatically construct an entailment graph from source sentences. Finally, by swapping source and target sentences we can also train a model that given an input sentence invents additional information to generate a new sentence.

1 Introduction

The ability to determine entailment or contradiction between natural language text is essential for improving the performance in a wide range of natural language processing tasks. Recognizing Textual Entailment (RTE) is a task primarily designed to determine whether two natural language sentences are independent, contradictory or in an entailment relationship where the second sentence (the hypothesis) can be inferred from the first (the premise). Although systems that perform well in RTE could potentially be used to improve question answering, information extraction, text summarization and machine translation [6], only in few of such downstream NLP tasks sentence-pairs are actually available. Usually, only a single source sentence (*e.g.* a question that needs to be answered or a source sentence that we want to translate) is present and models need to come up with their own hypotheses and commonsense knowledge inferences.

The release of the large Stanford Natural Language Inference (SNLI) corpus [2] allowed end-to-end differentiable neural networks to outperform feature-based classifiers on the RTE task [3, 4, 12, 15, 17].

In this work, we go a step further and investigate how well recurrent neural networks can produce true hypotheses given a source sentence. Furthermore, we qualitatively demonstrate that by only training on input-output pairs and recursively generating entailed sentence we can generate natural language inference chains (see Figure 1 for an example). Note that every inference step is interpretable as it is mapping one natural language sentence to another one.

Our contributions are fourfold: (i) we propose

The Renewed Case for the Reduced Instruction Set Computer: Avoiding ISA Bloat with Macro-Op Fusion for RISC-V

Christopher Celio, Palmer Dabbelt, David Patterson, Krste Asanović
Department of Electrical Engineering and Computer Sciences, University of California, Berkeley
celio@eecs.berkeley.edu

***Abstract*—This report makes the case that a well-designed Reduced Instruction Set Computer (RISC) can match, and even exceed, the performance and code density of existing commercial Complex Instruction Set Computers (CISC) while maintaining the simplicity and cost-effectiveness that underpins the original RISC goals [12].**

We begin by comparing the dynamic instruction counts and dynamic instruction bytes fetched for the popular proprietary ARMv7, ARMv8, IA-32, and x86-64 Instruction Set Architectures (ISAs) against the free and open RISC-V RV64G and RV64GC ISAs when running the SPEC CINT2006 benchmark suite. RISC-V was designed as a very small ISA to support a wide range of implementations, and has a less mature compiler toolchain. However, we observe that on SPEC CINT2006 RV64G executes on average 16% more instructions than x86-64, 3% more instructions than IA-32, 9% more instructions than ARMv8, but 4% fewer instructions than ARMv7.

CISC x86 implementations break up complex instructions into smaller internal RISC-like *micro-ops*, and the RV64G instruction count is within 2% of the x86-64 retired micro-op count. RV64GC, the compressed variant of RV64G, is the densest ISA studied, fetching 8% fewer dynamic instruction bytes than x86-64. We observed that much of the increased RISC-V instruction count is due to a small set of common multi-instruction idioms.

Exploiting this fact, the RV64G and RV64GC *effective instruction* count can be reduced by 5.4% on average by leveraging *macro-op fusion*. Combining the compressed RISC-V ISA extension with macro-op fusion provides both the densest ISA and the fewest dynamic operations retired per program, reducing the motivation to add more instructions to the ISA. This approach retains a single simple ISA suitable for both low-end and high-end implementations, where high-end implementations can boost performance through microarchitectural techniques.

Compiler tool chains are a continual work-in-progress, and the results shown are a snapshot of the state as of July 2016 and are subject to change.

I. Introduction

The Instruction Set Architecture (ISA) specifies the set of instructions that a processor must understand and the expected effects of each instruction. One of the goals of the RISC-V project was to produce an ISA suitable for a wide range of implementations from tiny microcontrollers to the largest supercomputers [14]. Hence, RISC-V was designed with a much smaller number of simple standard instructions compared to other popular ISAs, including other RISC-inspired ISAs. A simple ISA is clearly a benefit for a small resource-constrained microcontroller, but how much performance is lost for high-performance implementations by not supporting the numerous instruction variants provided by popular proprietary ISAs?

A casual observer might argue that a processor's performance increases when it executes fewer instructions for a given program, but in reality, the performance is more accurately described by the Iron Law of Performance [8]:

$$\frac{seconds}{program} = \frac{cycles}{instruction} * \frac{seconds}{cycle} * \frac{instructions}{program}$$

The ISA is just an abstract boundary; behind the scenes the processor may choose to implement instructions in any number of ways that trade off $\frac{cycles}{instruction}$, or *CPI*, and $\frac{seconds}{cycle}$, or *frequency*.

For example, a fairly powerful x86 instruction is the *repeat move* instruction (`rep movs`), which copies *C* bytes of data from one memory location to another:

```
// psuedo-code for a 'repeat move' instruction
for (i=0; i < C; i++)
   d[i] = s[i];
```

Implementations of the x86 ISA break up the *repeat move* instruction into smaller operations, or *micro-ops*, that individually perform the required operations of loading the data from the old location, storing the data to the new location, incrementing the address pointers, and checking to see if the end condition has been met. Therefore, a raw comparison of instruction counts may hide a significant amount of work and complexity to execute a particular benchmark.

In contrast to the process of generating many micro-ops from a single ISA instruction, several commercial microprocessors perform *macro-op fusion*, where several ISA instructions are fused in the decode stage and handled as one internal operation. As an example, compare-and-branch is a very commonly executed idiom, and the RISC-V ISA includes a full register-register magnitude comparison in its branch instructions. However, both ARM and x86 typically require two ISA instructions to specify a compare-and-branch. The first instruction performs the *comparison* and sets a condition code, and the second instruction performs the *jump-on-condition-code*. While it would seem that ARM and x86 would have a penalty of one additional instruction on nearly every loop compared to RISC-V, the reality is more complicated. Both ARM and Intel employ the technique of macro-op fusion, in which the processor front-end detects these two-instruction compare-and-branch sequences in the instruction stream and "fuses" them together into a single *macro-op*, which can then be handled as a single compare-and-branch instruction by the processor back-end to reduce the effective dynamic instruction count.[1]

[1]The reality can be even more complicated. Depending on the micro-architecture, the front-end may fuse the two instructions together to save decode, allocation, and commit bandwidth, but break them apart in the execution pipeline for critical path or complexity reasons [6].

THE MICROSOFT 2016 CONVERSATIONAL SPEECH RECOGNITION SYSTEM

W. Xiong, J. Droppo, X. Huang, F. Seide, M. Seltzer, A. Stolcke, D. Yu and G. Zweig

Microsoft Research

ABSTRACT

We describe Microsoft's conversational speech recognition system, in which we combine recent developments in neural-network-based acoustic and language modeling to advance the state of the art on the Switchboard recognition task. Inspired by machine learning ensemble techniques, the system uses a range of convolutional and recurrent neural networks. I-vector modeling and lattice-free MMI training provide significant gains for all acoustic model architectures. Language model rescoring with multiple forward and backward running RNNLMs, and word posterior-based system combination provide a 20% boost. The best single system uses a ResNet architecture acoustic model with RNNLM rescoring, and achieves a word error rate of 6.9% on the NIST 2000 Switchboard task. The combined system has an error rate of 6.2%, representing an improvement over previously reported results on this benchmark task.

Index Terms— Conversational speech recognition, convolutional neural networks, recurrent neural networks, VGG, ResNet, LACE, BLSTM.

1. INTRODUCTION

Recent years have seen a rapid reduction in speech recognition error rates as a result of careful engineering and optimization of convolutional and recurrent neural networks. While the basic structures have been well known for a long period [1, 2, 3, 4, 5, 6, 7], it is only recently that they have dominated the field as the best models for speech recognition. Surprisingly, this is the case for both acoustic modeling [8, 9, 10, 11, 12, 13] and language modeling [14, 15]. In comparison to standard feed-forward MLPs or DNNs, these acoustic models have the ability to model a large amount of acoustic context with temporal invariance, and in the case of convolutional models, with frequency invariance as well. In language modeling, recurrent models appear to improve over classical N-gram models through the generalization ability of continuous word representations [16]. In the meantime, ensemble learning has become commonly used in several neural models [17, 18, 15], to improve robustness by reducing bias and variance.

In this paper, we use ensembles of models extensively, as well as improvements to individual component models, to to advance the state-of-the-art in conversational telephone speech recognition (CTS), which has been a benchmark speech recognition task since the 1990s. The main features of this system are:

1. An ensemble of two fundamental acoustic model architectures, convolutional neural nets (CNNs) and long-short-term memory nets (LSTMs), with multiple variants of each
2. An attention mechanism in the LACE CNN which differentially weights distant context [19]
3. Lattice-free MMI training [20, 21]
4. The use of i-vector based adaptation [22] in all models
5. Language model (LM) rescoring with multiple, recurrent neural net LMs [14] running in both forward and reverse direction
6. Confusion network system combination [23] coupled with search for best system subset, as necessitated by the large number of candidate systems.

The remainder of this paper describes our system in detail. Section 2 describes the CNN and LSTM models. Section 3 describes our implementation of i-vector adaptation. Section 4 presents out lattice-free MMI training process. Language model rescoring is a significant part of our system, and described in Section 5. Experimental results are presented in Section 6, followed by a discussion of related work and conclusions.

2. CONVOLUTIONAL AND LSTM NEURAL NETWORKS

We use three CNN variants. The first is the VGG architecture of [24]. Compared to the networks used previously in image recognition, this network uses small (3x3) filters, is deeper, and applies up to five convolutional layers before pooling. The second network is modeled on the ResNet architecture [25], which adds highway connections [26], i.e. a linear transform of each layer's input to the layer's output [26, 27]. The only difference is that we move the Batch Normalization node to the place right before each ReLU activation.

The last CNN variant is the LACE (layer-wise context expansion with attention) model [19]. LACE is a TDNN [3] variant in which each higher layer is a weighted sum of nonlinear transformations of a window of lower layer frames. In other words, each higher layer exploits broader context than lower layers. Lower layers focus on extracting simple local patterns while higher layers extract complex patterns that cover broader contexts. Since not all frames in a window carry the same importance, an attention mask is applied. The LACE model differs from the earlier TDNN models e.g. [3, 28] in the use of a learned attention mask and ResNet like linear pass-through. As illustrated in detail in Figure 1, the model is composed of 4 blocks, each with the same architecture. Each block starts with a convolution layer with stride 2 which sub-samples the input and increases the number of channels. This layer is followed by 4 RELU-convolution layers with jump links similar to those used in ResNet. Table 1 compares the layer structure and parameters of the three CNN architectures.

While our best performing models are convolutional, the use of long short-term memory networks is a close second. We use a bidirectional architecture [29] without frame-skipping [9]. The core model structure is the LSTM defined in [8]. We found that using networks with more than six layers did not improve the word error rate on the development set, and chose 512 hidden units, per direction, per layer, as that provided a reasonable trade-off between training time and final model accuracy. Network parameters for different configurations of the LSTM architecture are summarized in Table 2.

Quantum-Chemical Insights from Deep Tensor Neural Networks

Kristof T. Schütt[1], Farhad Arbabzadah[1], Stefan Chmiela[1], Klaus R. Müller[1,2,*] and Alexandre Tkatchenko[3,4†]
[1]*Machine Learning Group, Technische Universität Berlin, Marchstr. 23, 10587 Berlin, Germany*
[2]*Department of Brain and Cognitive Engineering, Korea University, Anam-dong, Seongbuk-gu, Seoul 136-713, Republic of Korea*
[3]*Fritz-Haber-Institut der Max-Planck-Gesellschaft, Faradayweg 4-6, D-14195, Berlin, Germany*
[4]*Physics and Materials Science Research Unit, University of Luxembourg, L-1511 Luxembourg*

Learning from data has led to paradigm shifts in a multitude of disciplines, including web, text, and image search, speech recognition, as well as bioinformatics. Can machine learning spur similar breakthroughs in understanding quantum many-body systems? Here we develop an efficient deep learning approach that enables spatially and chemically resolved insights into quantum-mechanical observables of molecular systems. We unify concepts from many-body Hamiltonians with purpose-designed deep tensor neural networks (DTNN), which leads to size-extensive and uniformly accurate (1 kcal/mol) predictions in compositional and configurational chemical space for molecules of intermediate size. As an example of chemical relevance, the DTNN model reveals a classification of aromatic rings with respect to their stability – a useful property that is not contained as such in the training dataset. Further applications of DTNN for predicting atomic energies and local chemical potentials in molecules, reliable isomer energies, and molecules with peculiar electronic structure demonstrate the high potential of machine learning for revealing novel insights into complex quantum-chemical systems.

Chemistry permeates all aspects of our life, from the development of new drugs to the food that we consume and materials we use on a daily basis. Chemists rely on empirical observations based on creative and painstaking experimentation that leads to eventual discoveries of molecules and materials with desired properties and mechanisms to synthesize them. Many discoveries in chemistry can be guided by searching large databases of experimental or computational molecular structures and properties by using concepts based on chemical similarity. Because the structure and properties of molecules are determined by the laws of quantum mechanics, ultimately chemical discovery must be based on fundamental quantum principles. Indeed, electronic structure calculations and intelligent data analysis (machine learning, ML) have recently been combined aiming towards the goal of accelerated discovery of chemicals with desired properties [1–8]. However, so far the majority of these pioneering efforts have focused on the construction of reduced models trained on large datasets of density-functional theory calculations. In this work, we develop an efficient deep learning approach that enables spatially and chemically resolved insights into quantum-mechanical properties of molecular systems beyond those trivially contained in the training dataset. Obviously, computational models are not predictive if they lack accuracy. In addition to being interpretable, size extensive and efficient, our deep tensor neural network (DTNN) approach is uniformly accurate (1 kcal/mol) throughout compositional and configurational chemical space. On the more fundamental side, the mathematical construction of the DTNN model provides statistically rigorous partitioning of extensive molecular properties into atomic contributions – a long-standing challenge for quantum-mechanical calculations of molecules.

MOLECULAR DEEP TENSOR NEURAL NETWORKS

It is common to use a carefully chosen representation of the problem at hand as a basis for machine learning [9–11]. For example, molecules can be represented as Coulomb matrices [7, 12, 13], scattering transforms [14], bags of bonds (BoB) [15], smooth overlap of atomic positions (SOAP) [16, 17], or generalized symmetry functions [18, 19]. Kernel-based learning of molecular properties transforms these representations non-linearly by virtue of kernel functions. In contrast, deep neural networks [20] are able to infer the underlying regularities and learn an efficient representation in a layer-wise fashion [21].

Molecular properties are governed by the laws of quantum mechanics, which yield the remarkable flexibility of chemical systems, but also impose constraints on the behavior of bonding in molecules. The approach presented here utilizes the many-body Hamiltonian concept for the construction of the DTNN architecture (see Fig. 1), embracing the principles of quantum chemistry, while maintaining the full flexibility of a complex data-driven learning machine.

DTNN receives molecular structures through a vector of nuclear charges Z and a matrix of atomic distances D ensuring rotational and translational invariance by construction (Fig. 1A). The distances are expanded in a Gaussian basis, yielding a feature vector $\hat{\mathbf{d}}_{ij}$, which accounts for the different nature of interactions at various distance regimes.

The total energy E_M for the molecule M composed of N atoms is written as a sum over N atomic energy contributions E_i, thus satisfying permutational invariance with respect to atom indexing. Each atom i is represented by a coefficient vector $\mathbf{c} \in \mathbb{R}^B$, where B is the number of basis functions, or features. Motivated by quantum-chemical atomic basis set expansions, we assign an atom type-specific descriptor vector $\mathbf{c}_{Z_i}$ to these coefficients $\mathbf{c}_i^{(0)}$. Subsequently, this atomic expansion is repeatedly refined by pairwise interactions with the

A computer program for simulating time travel and a possible 'solution' for the grandfather paradox

Doron Friedman, The Interdisciplinary Center, Herzliya, Israel

doronf@idc.ac.il

Abstract

While the possibility of time travel in physics is still debated, the explosive growth of virtual-reality simulations opens up new possibilities to rigorously explore such time travel and its consequences in the digital domain. Here we provide a computational model of time travel and a computer program that allows exploring digital time travel. In order to explain our method we formalize a simplified version of the famous grandfather paradox, show how the system can allow the participant to go back in time, try to kill their ancestors before they were born, and experience the consequences. The system has even come up with scenarios that can be considered consistent "solutions" of the grandfather paradox. We discuss the conditions for digital time travel, which indicate that it has a large number of practical applications.

1. Introduction

In the principal paradox of time travel a person travels back in time and kills his grandfather before the grandfather meets the time traveler's grandmother. As a consequence, one of the traveler's parents, and therefore the traveler himself, would never have been born. This would imply that the traveller could not have travelled back in time, which means that the grandfather would still be alive, which now makes it possible for the traveler to be born, travel back in time and kill his grandfather, hence a paradox.

In this paper we describe a computer program that allows us to interactively explore the consequences of "changing the past" in a narrative. Our system uses well-known techniques from automated reasoning to compute the specific consequences of modifying history. The contribution of this paper is in the application of automated reasoning to the experience of time travel and in the implementation of this method in a computer

HYPERNETWORKS

David Ha[*], **Andrew Dai, Quoc V. Le**
Google Brain
{hadavid,adai,qvl}@google.com

ABSTRACT

This work explores hypernetworks: an approach of using a one network, also known as a hypernetwork, to generate the weights for another network. Hypernetworks provide an abstraction that is similar to what is found in nature: the relationship between a genotype – the hypernetwork – and a phenotype – the main network. Though they are also reminiscent of HyperNEAT in evolution, our hypernetworks are trained end-to-end with backpropagation and thus are usually faster. The focus of this work is to make hypernetworks useful for deep convolutional networks and long recurrent networks, where hypernetworks can be viewed as relaxed form of weight-sharing across layers. Our main result is that hypernetworks can generate non-shared weights for LSTM and achieve near state-of-the-art results on a variety of sequence modelling tasks including character-level language modelling, handwriting generation and neural machine translation, challenging the weight-sharing paradigm for recurrent networks. Our results also show that hypernetworks applied to convolutional networks still achieve respectable results for image recognition tasks compared to state-of-the-art baseline models while requiring fewer learnable parameters.

1 INTRODUCTION

In this work, we consider an approach of using a small network (called a "hypernetwork") to generate the weights for a larger network (called a main network). The behavior of the main network is the same with any usual neural network: it learns to map some raw inputs to their desired targets; whereas the hypernetwork takes a set of inputs that contain information about the structure of the weights and generates the weight for that layer (see Figure 1).

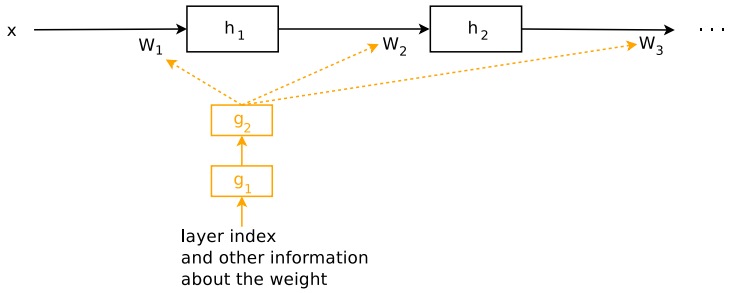

Figure 1: A hypernetwork generates the weights for a feedforward network. Black connections and parameters are associated the main network whereas orange connections and parameters are associated with the hypernetwork.

HyperNEAT (Stanley et al., 2009) is an example of hypernetworks where the inputs are a set of virtual coordinates for each weight in the main network. In this work, we will focus on a more powerful approach where the input is an embedding vector that describes the entire weights of a given layer. Our embedding vectors can be fixed parameters that are also learned during end-to-end training, allowing approximate weight-sharing within a layer and across layers of the main network. In

[*]Work done as a member of the Google Brain Residency program (g.co/brainresidency).

A low-cost, Arduino-like development kit for single-element ultrasound imaging*

Luc Jonveaux[1]

***Abstract*— An open-source software ecosystem for ultrasound imaging is widely available to developers, however, limited resources can be found on the open-hardware side. The focus of this work was to develop an easy-to-use platform kit (hardware and software) for providing the community a complete experimental setup for ultrasound imaging at a low cost, without the need of specific equipment. The goal of this work resembles the needs of medical systems in the 80's where analog techniques using single-sensor devices were prominent.**

To this end, two open-source, arduino-like modules have been developed for building a simple, yet complete, single-channel analog front-end system, where all the intermediary signals are readily accessible by the user. A single-channel architecture avoids the beamforming overhead, though it limits the quality of the captured image, and brings simplicity to the system.

The modules were tested using re-purposed ultrasound mechanical probes, as well as non-medical transducers. Furthermore, different digital acquisition systems were utilized for providing the images of interest. The developed modules can also be used in Radio Frequency (RF) projects, non-destructive testing and control projects, as well as in low-cost medical imaging projects.

I. Introduction

A. Approach

Ultrasound imaging has evolved since the first ultrasound machine appeared. The first devices were using single-sensor (transducers) techniques, coupled with mechanical scanning [22]. The architecture of such systems, as shown in Fig. 1, is well-known and formed the basis of ultrasound imaging.

Mechanical scanning has its limitation, but also its strengths: a single signal channel, linked to a single sensor, means that the corresponding electronics are simplified, and the cost is reduced. Moreover, with progress made in different technical fields, mechanical probes are seen on the market again. Search in academic literature, and open-electronics resources, yielded little to no documentation of previous research to rebuild these mechanical ultrasound imaging devices.

To the best of the author's knowledge, there are no open-source hardware designs nor electronics accessible online for the analog-processing component. To bridge this gap, this work provides modules to the community to understand and recreate the electronic core of an ultrasound device.

B. This work

This kit consists of several modules mainly built from easily available components. **Two electronic modules were specifically designed to provide the basic development kit**. These two modules, called the Ultrasound Imaging Analog Core (UIAC), as shown in Fig. 1, are:

- the **Transducer Pulser Module (TPM)**: designed to provide a precise high-voltage pulse, necessary to excite the sensor, while remaining robust enough to be controlled by an Arduino;
- the **Analog Processing Module (APM)**: designed to correctly process the raw ultrasound electric signal, while easily exposing all intermediary signals, and exposing a digital output to the user.

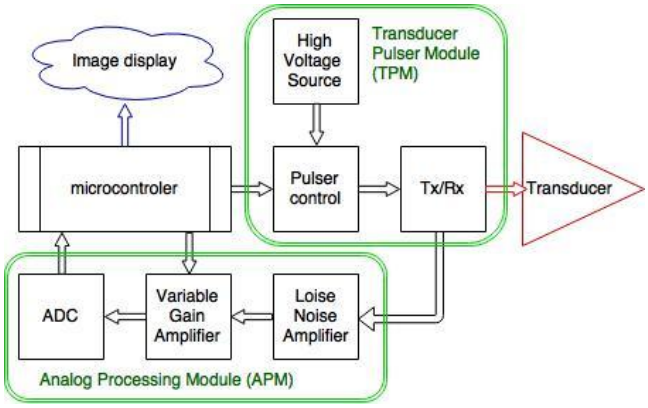

Fig. 1. Architecture of the ultrasound imaging system. The two custom boards, TPM and APM, are shown in green.

C. A module approach

We have chosen a modular approach to ensure that each key component inside the ultrasound image processing can easily be replaced and compared with another module. Each electronic module takes the place of a function in the signal processing chain or allows tapping into the different signals circulating between the blocks.

We have considered readily available open-source modules and recycled components (probes) to provide the user with building bricks for the basic non-medical ultrasound imaging tool.

We remind that the aim of this work is not to design an ultrasound probe: *the goal of the present article is rather to provide a basic open-source tool to understand ultrasound imaging technique and provide the analog core, unavailable today, as well as selecting proper off-the-shelf components for the other elements*.

This paper also discusses several possible options, keeping in mind that none are preferred and that the modular

*This work was not supported by any organization

[1]Luc is just a independant maker, reachable at kelu124 at gmail.com

Strong Federations: An Interoperable Blockchain Solution to Centralized Third-Party Risks

Johnny Dilley*, Andrew Poelstra*, Jonathan Wilkins*, Marta Piekarska*, Ben Gorlick*, and Mark Friedenbach*
Email: johnny, andrew, jonathan, marta, ben, mark @blockstream.com

***Abstract*—Bitcoin, the first peer-to-peer electronic cash system, opened the door to permissionless, private, and trustless transactions. Attempts to repurpose Bitcoin's underlying blockchain technology have run up against fundamental limitations to privacy, faithful execution, and transaction finality. We introduce *Strong Federations*: publicly verifiable, Byzantine-robust transaction networks that facilitate movement of any asset between disparate markets, without requiring third-party trust. *Strong Federations* enable commercial privacy, with support for transactions where asset types and amounts are opaque, while remaining publicly verifiable. As in Bitcoin, execution fidelity is cryptographically enforced; however, *Strong Federations* significantly lower capital requirements for market participants by reducing transaction latency and improving interoperability. To show how this innovative solution can be applied today, we describe *Liquid*: the first implementation of *Strong Federations* deployed in a Financial Market.**

I. Introduction

Bitcoin, proposed by Satoshi Nakamoto in 2008, is based on the idea of a *blockchain* [1]. A blockchain consists of a series of blocks, each of which is composed of time-stamped sets of transactions and a hash of the previous block, which connects the two together, as presented in Figure 1.

The underlying principle of Bitcoin's design is that all participants in its network are on equal footing. They jointly trust proof-of-work [2] to validate and enforce the network's rules, which obviates the need for central authorities such as clearinghouses. As a result, Bitcoin empowers a wide range of participants to be their own banks – storing, transacting, and clearing for themselves without the need for a third-party intermediary. Bitcoin's network automatically enforces settlements between participants using publicly verifiable algorithms that avoid security compromises, expensive (or unavailable) legal infrastructure, third-party trust requirements, or the physical transportation of money. For the first time, users of a system have the ability to cryptographically verify other participants' behaviors, enforcing rules based on mathematics that anyone can check and no one can subvert.

Due to its design, Bitcoin has characteristics that make it a vehicle of value unlike anything that previously existed. First, it eliminates most counterparty risk from transactions [3]. Second, it offers cryptographic proof of ownership of assets, as the knowledge of a cryptographic key defines ownership [4]. Third, it is a programmable asset, offering the ability to pay to a program, or a "smart contract", rather than a passive account or a singular public key [5]. Fourth, and finally, it is a disruptive market mechanism for use cases such as point-to-point real-time transfers, accelerated cross-border payment, B2B remittance, asset transfers, and micropayments [6].

A. Problem Statement

Because it is a global consensus system, Bitcoin's decentralized network and public verifiability come with costs. Speed of execution and insufficient guarantees of privacy are two of Bitcoin's limitations.

Bitcoin's proof-of-work methodology was designed to process transactions on average only once every ten minutes, with large variance. As a result, Bitcoin is slow from a real-time transaction processing perspective. This creates spontaneous illiquidity for parties using bitcoin[1] as an intermediary, volatility exposure for those holding bitcoin for any length of time, and obstacles for the use of Bitcoin's contracting features for fast settlements. Even after a transaction is processed, counterparties must generally wait until several additional blocks have been created before considering their transaction settled. This is because Bitcoin's global ledger is at constant risk of *reorganization*, wherein very recent history can be modified or rewritten. This latency undermines many commercial applications, which require real-time, or nearly instant, execution[2]. Today, solving this requires a centralized counterparty, which introduces a third-party risk.

Despite issues of short-term validation, Bitcoin excels on settlement finality, providing strong assurance against transaction reversals after adequate block confirmations. In contrast, legacy payment networks leave absolute final settlement in limbo for up to 120 days typically, though chargebacks have been allowed up to 8 years late [7], depending on policies imposed by the centralized network owner [8] [9].

While a popular prevailing belief is that Bitcoin is anonymous [10], its privacy properties are insufficient for many commercial use cases. Every transaction is published in a global ledger, which allows small amounts of information about users' financial activity (e.g., the identities of the participants in a single transaction [11]) to be amplified by statistical analysis [12]. This limits the commercial usefulness of the network and also harms individual privacy [13], as user behavior frequently reflects the pervasive assumption that Bitcoin is an anonymous system. Further, it can damage the

[1]The capitalized "Bitcoin" is used to talk about the technology and the engine, while the lowercase "bitcoin" is used to refer to the currency.

[2]In most traditional systems, the speed of transaction is achieved by instant execution and delayed settlement.

Draft version February 28, 2017
Typeset using LaTeX **twocolumn** style in AASTeX61

FAST RADIO BURSTS FROM EXTRAGALACTIC LIGHT SAILS

Manasvi Lingam[1,2] and Abraham Loeb[2]

[1] *Harvard John A. Paulson School of Engineering and Applied Sciences, Harvard University, Cambridge, MA 02138, USA*
[2] *Harvard-Smithsonian Center for Astrophysics, The Institute for Theory and Computation, 60 Garden Street, Cambridge, MA 02138, USA*

ABSTRACT

We examine the possibility that Fast Radio Bursts (FRBs) originate from the activity of extragalactic civilizations. Our analysis shows that beams used for powering large light sails could yield parameters that are consistent with FRBs. The characteristic diameter of the beam emitter is estimated through a combination of energetic and engineering constraints, and both approaches intriguingly yield a similar result which is on the scale of a large rocky planet. Moreover, the optimal frequency for powering the light sail is shown to be similar to the detected FRB frequencies. These 'coincidences' lend some credence to the possibility that FRBs might be artificial in origin. Other relevant quantities, such as the characteristic mass of the light sail, and the angular velocity of the beam, are also derived. By using the FRB occurrence rate, we infer upper bounds on the rate of FRBs from extragalactic civilizations in a typical galaxy. The possibility of detecting fainter signals is briefly discussed, and the wait time for an exceptionally bright FRB event in the Milky Way is estimated.

Corresponding author: Manasvi Lingam
manasvi@seas.harvard.edu

INCREMENTAL NETWORK QUANTIZATION: TOWARDS LOSSLESS CNNS WITH LOW-PRECISION WEIGHTS

Aojun Zhou*, **Anbang Yao, Yiwen Guo, Lin Xu, and Yurong Chen**
Intel Labs China
{aojun.zhou, anbang.yao, yiwen.guo, lin.x.xu, yurong.chen}@intel.com

ABSTRACT

This paper presents incremental network quantization (INQ), a novel method, targeting to efficiently convert any pre-trained full-precision convolutional neural network (CNN) model into a low-precision version whose weights are constrained to be either powers of two or zero. Unlike existing methods which are struggled in noticeable accuracy loss, our INQ has the potential to resolve this issue, as benefiting from two innovations. On one hand, we introduce three interdependent operations, namely weight partition, group-wise quantization and re-training. A well-proven measure is employed to divide the weights in each layer of a pre-trained CNN model into two disjoint groups. The weights in the first group are responsible to form a low-precision base, thus they are quantized by a variable-length encoding method. The weights in the other group are responsible to compensate for the accuracy loss from the quantization, thus they are the ones to be re-trained. On the other hand, these three operations are repeated on the latest re-trained group in an iterative manner until all the weights are converted into low-precision ones, acting as an incremental network quantization and accuracy enhancement procedure. Extensive experiments on the ImageNet classification task using almost all known deep CNN architectures including AlexNet, VGG-16, GoogleNet and ResNets well testify the efficacy of the proposed method. Specifically, at 5-bit quantization (a variable-length encoding: 1 bit for representing zero value, and the remaining 4 bits represent at most 16 different values for the powers of two) [1], our models have improved accuracy than the 32-bit floating-point references. Taking ResNet-18 as an example, we further show that our quantized models with 4-bit, 3-bit and 2-bit ternary weights have improved or very similar accuracy against its 32-bit floating-point baseline. Besides, impressive results with the combination of network pruning and INQ are also reported. We believe that our method sheds new insights on how to make deep CNNs to be applicable on mobile or embedded devices. The code is available at https://github.com/Zhouaojun/Incremental-Network-Quantization.

1 INTRODUCTION

Deep convolutional neural networks (CNNs) have demonstrated record breaking results on a variety of computer vision tasks such as image classification (Krizhevsky et al., 2012; Simonyan & Zisserman, 2015), face recognition (Taigman et al., 2014; Sun et al., 2014), semantic segmentation (Long et al., 2015; Chen et al., 2015a) and object detection (Girshick, 2015; Ren et al., 2015). Regardless of the availability of significantly improved training resources such as abundant annotated data, powerful computational platforms and diverse training frameworks, the promising results of deep CNNs are mainly attributed to the large number of learnable parameters, ranging from tens of millions to even hundreds of millions. Recent progress further shows clear evidence that CNNs could easily enjoy the accuracy gain from the increased network depth and width (He et al., 2016; Szegedy et al., 2015; 2016). However, this in turn lays heavy burdens on the memory and

*This work was done when Aojun Zhou was an intern at Intel Labs China, supervised by Anbang Yao who proposed the original idea and is responsible for correspondence. The first three authors contributed equally to the writing of the paper.

[1]This notation applies to our method throughout the paper.

Protein bioelectronics: a review of what we do and do not know

Christopher D. Bostick,[#1,2] Sabyasachi Mukhopadhyay,[#3‡] Israel Pecht,[3*] Mordechai Sheves,[3*] David Cahen,[3*] David Lederman*[4]

[1] *Dept. of Pharmaceutical Sciences, West Virginia University, Morgantown, WV 26506, USA*

[2] *Inst. for Genomic Medicine, Columbia University Medical Center, New York, NY 10032, USA*

[3] *Departments of Materials & Interfaces, of Organic Chemistry and of Immunology, Weizmann Institute of Science, Rehovot, Israel 76100*

[4] *Department of Physics, University of California, Santa Cruz, CA 95060, USA*

[#] These authors contributed equally to the work

* Corresponding authors, email addresses: david.cahen@weizmann.ac.il, dlederma@ucsc.edu, mudi.sheves@weizmann.ac.il, israel.pecht@weizmann.ac.il

Abstract

We review the status of protein-based molecular electronics. First, we define and discuss fundamental concepts of electron transfer and transport in and across proteins and proposed mechanisms for these processes. We then describe the immobilization of proteins to solid-state surfaces in both nanoscale and macroscopic approaches, and highlight how different methodologies can alter protein electronic properties. Because immobilizing proteins while retaining biological activity is crucial to the successful development of bioelectronic devices, we discuss this process at length. We briefly discuss computational predictions and their connection to experimental results. We then summarize how the biological activity of immobilized proteins is beneficial for bioelectronic devices, and how conductance measurements can shed light on protein properties. Finally, we consider how the research to date could influence the development of future bioelectronic devices.

[‡] Current affiliation - Department of Physics, School of Engineering & Applied Sciences, SRM University-AP, Amaravati, Andhra Pradesh, India - 522502

Sprites: Payment Channels that Go Faster than Lightning

Andrew Miller — *UIUC*
Iddo Bentov — *Cornell University*
Ranjit Kumaresan — *Microsoft Research*
Patrick McCorry — *Newcastle University*

Abstract

It is well known that Bitcoin, Ethereum, and other blockchain-based cryptocurrencies are facing hurdles in scaling to meet user demand. One of the most promising approaches is to form a network of "off-chain payment channels," which are backed by on-chain currency but support rapid, optimistic transactions and use the blockchain only in case of disputes.

We develop a novel construction for payment channels that reduces the worst-case "collateral cost" for off-chain payments. In existing proposals, particularly the Lightning Network, a payment across a path of ℓ channels requires locking up collateral for $O(\ell\Delta)$ time, where Δ is the time to commit a on-chain transaction. Our construction reduces this cost to $O(\ell+\Delta)$. We formalize our construction in the simulation-based security model, and provide an implementation as an Ethereum smart contract. Our construction relies on a general purpose primitive called a "state channel," which is of independent interest.

1 Introduction

Cryptocurrencies such as Bitcoin, Ethereum, and others, derive their security from wide replication, which unfortunately comes at the expense of limited scalability. A leading proposal for improved scaling of cryptocurrencies is to form a network of "off-chain" rapid payment channels, which act like credit lines secured by "on-chain" currency. In this vision of the future, cryptocurrencies will largely be used as collateral, so interaction with the blockchain directly will rarely be needed.

A chief concern for the feasibility of payment networks is whether the "collateral costs" will be prohibitive. In general, collateral cost is the lost opportunity (in dimensions of money $\times$ time) occurring when funds are held in escrow instead of being invested profitably. Currency deposited in a payment channel can earn fees when it is used to facilitate linked payments. However, each in-flight payment along a channel must reserve a portion of that channel's available collateral, preventing its use elsewhere until the payment is settled. In the optimistic case, payments complete quickly, requiring only off-chain point-to-point messages; but if some party fails, the collateral can be tied up for a significant duration, until the balance can be settled on-chain. The more hops in a payment path, the more collateral must

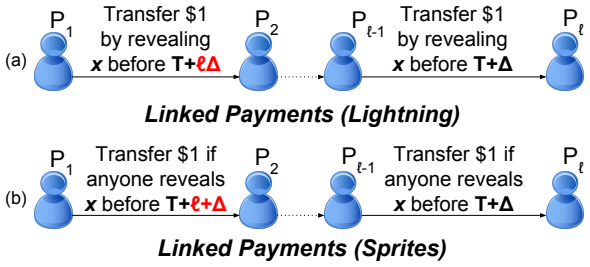

Figure 1: Cryptocurrencies like Bitcoin and Ethereum can serve as collateral for a scalable payment network (i.e. a credit network without counterparty risk) [26, 8]. Payment channels (a) let one party rapidly pay another using available collateral, requiring a blockchain transaction only in case of dispute. Payments across multiple channels (b) can be linked using a common condition (such as revealing the preimage of a hash, h). We contribute a novel payment channel (c) improving the worst case delay for ℓ-hop payments from $O(\ell\Delta)$ to $O(\ell+\Delta)$.

be reserved: $O(\ell\$X)$ in total for a $O(X)$ sized payment spanning ℓ channels. Furthermore, due to limitations of the current state-of-the-art payment channels, each link in the path adds an additional worst-case delay. This additional delay is determined by the worst-case confirmation time for an on-chain transaction, which we denote by Δ (i.e., an on-chain transaction may take Δ times longer than an ordinary off-chain message). Thus the worst-case delay is $O(\ell\Delta)$, and so the total collateral cost of a $\$X$ payment over a path of length ℓ is $O(\ell^2\$X\Delta)$.

In this paper we present an improved construction of payment channels, called "Sprites," that reduce the timeout delay from $O(\ell\Delta)$ to $O(\ell+\Delta)$, resulting in a total collateral cost of $O(\ell\$X\Delta)$ for a payment over ℓ hops. Our solution makes use of a feature available today in Ethereum smart contracts, but that cannot (we conjecture) be implemented in Bitcoin — in particular, the ability for a transaction to depend on a "global" event recorded in the blockchain.

Our construction is highly modular; a key contribution of our work is the development of a useful general primitive called a "state channel," which allows two or more parties to maintain an arbitrary off-chain shared process, which can be synchronized on demand (or in case of a dispute) with the blockchain. This abstraction neatly encapsulates the underlying cryptography; by making use of it, our payment channel constructions do not mention

Deep Forest: Towards an Alternative to Deep Neural Networks*

Zhi-Hua Zhou and **Ji Feng**
National Key Lab for Novel Software Technology, Nanjing University, Nanjing 210023, China
{zhouzh, fengj}@lamda.nju.edu.cn

Abstract

In this paper, we propose gcForest, a decision tree ensemble approach with performance highly competitive to deep neural networks in a broad range of tasks. In contrast to deep neural networks which require great effort in hyper-parameter tuning, gcForest is much easier to train; even when it is applied to different data across different domains in our experiments, excellent performance can be achieved by almost same settings of hyper-parameters. The training process of gcForest is efficient, and users can control training cost according to computational resource available. The efficiency may be further enhanced because gcForest is naturally apt to parallel implementation. Furthermore, in contrast to deep neural networks which require large-scale training data, gcForest can work well even when there are only small-scale training data.

1 Introduction

In recent years, deep neural networks have achieved great success in various applications, particularly in tasks involving visual and speech information [Krizhenvsky *et al.*, 2012; Hinton *et al.*, 2012], leading to the hot wave of deep learning [Goodfellow *et al.*, 2016].

Though deep neural networks are powerful, they have apparent deficiencies. First, it is well known that a huge amount of training data are usually required for training, disabling deep neural networks to be directly applied to tasks with small-scale data. Note that even in the big data era, many real tasks still lack sufficient amount of *labeled* data due to high cost of labeling, leading to inferior performance of deep neural networks in those tasks. Second, deep neural networks are very complicated models and powerful computational facilities are usually required for the training process, encumbering individuals outside big companies to fully exploit the learning ability. More importantly, deep neural networks are with too many hyper-parameters, and the learning performance depends seriously on careful tuning of them. For example, even when several authors all use convolutional neural networks [LeCun *et al.*, 1998; Krizhenvsky *et al.*, 2012; Simonyan and Zisserman, 2014], they are actually using different learning models due to the many different options such as the convolutional layer structures. This fact makes not only the training of deep neural networks very tricky, like an art rather than science/engineering, but also theoretical analysis of deep neural networks extremely difficult because of too many interfering factors with almost infinite configurational combinations.

It is widely recognized that the *representation learning* ability is crucial for deep neural networks. It is also noteworthy that, to exploit large training data, the capacity of learning models should be large; this partially explains why the deep neural networks are very complicated, much more complex than ordinary learning models such as support vector machines. We conjecture that if we can endow these properties to some other suitable forms of learning models, we may be able to achieve performance competitive to deep neural networks but with less aforementioned deficiencies.

In this paper, we propose gcForest (multi-Grained Cascade Forest), a novel decision tree ensemble method. This method generates a deep forest ensemble, with a cascade structure which enables gcForest to do representation learning. Its representational learning ability can be further enhanced by multi-grained scanning when the inputs are with high dimensionality, potentially enabling gcForest to be contextual or structural aware. The number of cascade levels can be adaptively determined such that the model complexity can be automatically set, enabling gcForest to perform excellently even on small-scale data. Moreover, users can control training costs according to computational resources available. The gcForest has much fewer hyper-parameters than deep neural networks; even better news is that its performance is quite robust to hyper-parameter settings, such that in most cases, even across different data from different domains, it is able to get excellent performance by using the default setting. This makes not only the training of gcForest convenient, but also theoretical analysis, although beyond the scope of this paper, potentially easier than deep neural networks (needless to say that tree learners are typically easier to analyze than neural networks). In our experiments, gcForest achieves highly competitive performance to deep neural networks, whereas the training time cost of gcForest is smaller than that of deep

*This research was supported by NSFC (61333014), 973 Program (2014CB340501) and the Collaborative Innovation Center of Novel Software Technology and Industrialization.

A Computational Model of Systems Memory Reconsolidation and Extinction

Peter Helfer and Thomas R. Shultz

McGill University

Enhancement of human color vision by breaking the binocular redundancy

Bradley S. Gundlach[1], Alireza Shahsafi[1], Gregory Vershbow[2], Chenghao Wan[1,3], Jad Salman[1], Bas Rokers[4,5], Laurent Lessard[1], Mikhail A. Kats[1,3,5*]

[1]Department of Electrical and Computer Engineering, University of Wisconsin-Madison
[2]Department of Art, University of Wisconsin-Madison
[3]Department of Materials Science and Engineering, University of Wisconsin-Madison
[4]Department of Psychology, University of Wisconsin-Madison
[5]McPherson Eye Research Institute, University of Wisconsin-Madison

*Corresponding Author: Mikhail A. Kats
Address: 1415 Engineering Dr, Madison, WI 53706
Email: mkats@wisc.edu
Phone: (608)890-3984

ABSTRACT

To see color, the human visual system combines the responses of three types of cone cells in the retina – a process that discards a significant amount of spectral information. We present an approach that can enhance human color vision by breaking the inherent redundancy in binocular vision, providing different spectral content to each eye. Using a psychophysical color model and thin-film optimization, we designed a wearable passive multispectral device that uses two distinct transmission filters, one for each eye, to enhance the user's ability to perceive spectral information. We fabricated and tested a design that "splits" the response of the short-wavelength cone of individuals with typical trichromatic vision, effectively simulating the presence of four distinct cone types between the two eyes ("tetrachromacy"). Users of this device were able to differentiate metamers (distinct spectra that resolve to the same perceived color in typical observers) without apparent adverse effects to vision. The increase in the number of effective cones from the typical three reduces the number of possible metamers that can be encountered, enhancing the ability to discriminate objects based on their emission, reflection, or transmission spectra. This technique represents a significant enhancement of the spectral perception of typical humans, and may have applications ranging from camouflage detection and anti-counterfeiting to art and data visualization.

Experimental certification of millions of genuinely entangled atoms in a solid

Florian Fröwis,* Peter C. Strassmann,† Alexey Tiranov,† Corentin Gut,‡ Jonathan Lavoie,§ Nicolas Brunner, Félix Bussières, Mikael Afzelius, and Nicolas Gisin
Groupe de Physique Appliquée, Université de Genève, CH-1211 Genève, Switzerland
(Dated: March 16, 2017)

Quantum theory predicts that entanglement can also persist in macroscopic physical systems, albeit difficulties to demonstrate it experimentally remain. Recently, significant progress has been achieved and genuine entanglement between up to 2900 atoms was reported. Here we demonstrate 16 million genuinely entangled atoms in a solid-state quantum memory prepared by the heralded absorption of a single photon. We develop an entanglement witness for quantifying the number of genuinely entangled particles based on the collective effect of directed emission combined with the nonclassical nature of the emitted light. The method is applicable to a wide range of physical systems and is effective even in situations with significant losses. Our results clarify the role of multipartite entanglement in ensemble-based quantum memories as a necessary prerequisite to achieve a high single-photon process fidelity crucial for future quantum networks. On a more fundamental level, our results reveal the robustness of certain classes of multipartite entangled states, contrary to, e.g., Schrödinger-cat states, and that the depth of entanglement can be experimentally certified at unprecedented scales.

A clear picture of large-scale entanglement with its complex structure is so far not developed. It is however important to understand the role of different facets of multipartite entanglement in nature and in technical applications [1, 2]. For example, the so-called Schrödinger cat states [3] are fundamentally different from a single photon coherently absorbed by a large atomic ensemble; even though both are instances of multipartite entanglement [4, chapter 16.5]. The theoretical study of large-scale entanglement has to be followed by an experimental demonstration, which consists of two basic steps: the preparation of an entangled system and a subsequent appropriate measurement verifying the presence of entanglement. In the context of entanglement in large systems, the preparation of entanglement is generally much simpler than its verification. For example, single-particle measurements are often not possible and collective measurements are typically restricted to certain types and are of finite resolution. These limitations call for new witnesses that allow one to certify entanglement based on accessible measurement data.

The concept of entanglement depth [5] was shown to be meaningful for and applicable to large quantum systems. It is defined as the smallest number of genuinely entangled particles that is compatible with the measured data. This allows one to witness at least one subgroup of genuinely entangled particles in a state-independent and scalable way. Large entanglement depth was successfully demonstrated with so-called spin-squeezed and oversqueezed states by measuring first and second moments of collective spin operators [6–9]; lately up of 680 atoms [10]. Recently, a witness was proposed that is designed for the W state, which is a coherent superposition of a single excitation shared by many atoms [11]. Based on this witness, an entanglement depth of around 2900 was measured [12]. However, these witnesses do not detect entanglement when the vacuum component of the state is dominant [11], even though the W state is known to be quite robust against various sources of noise, in particular, against loss of particles and excitation [13]. Hence, much larger values for the entanglement depth could be expected.

In this paper, we present theoretical methods and experimental data that verify a large entanglement depth in a solid-state quantum memory. A rare-earth-ion-doped crystal spectrally shaped to an atomic frequency comb (AFC) is used to absorb and re-emit light at the single-photon level [14–17], where at least 40 billion atoms collectively interact with the optical field. Using the measured photon number statistics of the re-emitted light we collect partial information about the quantum state of the atomic ensemble before emission. Then, we show that certain combinations of emission probabilities for one and two photons imply entanglement between a large number of atoms. With the measured data from our solid-state quantum memory we demonstrate inseparable groups of entangled particles containing at least 16 million atoms.

RESULTS

Before discussing the experiment, we give an intuitive explanation for the appearance of large entanglement depth when a large atomic ensemble coherently interacts with a single photon (see Fig. 1(a)). Suppose that N two-level atoms ($|g\rangle$ and $|e\rangle$ denote ground and excited state, respectively), couple to a light field. The quantised interaction in the dipole approximation is described by [18]

$$H_{\text{int}} = \sum_{j,\vec{k}} e^{-i\vec{k}\cdot\vec{r}_j} a_{\vec{k}} \sigma_+^{(j)} + e^{i\vec{k}\cdot\vec{r}_j} a_{\vec{k}}^\dagger \sigma_-^{(j)}, \qquad (1)$$

DEEP LSTM FOR LARGE VOCABULARY CONTINUOUS SPEECH RECOGNITION

Xu Tian, Jun Zhang, Zejun Ma, Yi He, Juan Wei, Peihao Wu, Wenchang Situ, Shuai Li, Yang Zhang

Alibaba Shenma Search, Beijing, China

{xu.tian, zj102217, zejun.mamzj, heyi.hy, wj80290, peihao.wph, wenchang.situwc, voolc.li, zy80232}@alibaba-inc.com

ABSTRACT

Recurrent neural networks (RNNs), especially long short-term memory (LSTM) RNNs, are effective network for sequential task like speech recognition. Deeper LSTM models perform well on large vocabulary continuous speech recognition, because of their impressive learning ability. However, it is more difficult to train a deeper network. We introduce a training framework with layer-wise training and exponential moving average methods for deeper LSTM models. It is a competitive framework that LSTM models of more than 7 layers are successfully trained on Shenma voice search data in Mandarin and they outperform the deep LSTM models trained by conventional approach. Moreover, in order for online streaming speech recognition applications, the shallow model with low real time factor is distilled from the very deep model. The recognition accuracy have little loss in the distillation process. Therefore, the model trained with the proposed training framework reduces relative 14% character error rate, compared to original model which has the similar real-time capability. Furthermore, the novel transfer learning strategy with segmental Minimum Bayes-Risk is also introduced in the framework. The strategy makes it possible that training with only a small part of dataset could outperform full dataset training from the beginning.

1. INTRODUCTION

Recently, deep neural network has been widely employed in various recognition tasks. Increasing the depth of neural network is a effective way to improve the performance, and convolutional neural network (CNN) has benefited from it in visual recognition task[1]. Deeper long short-term memory (LSTM) recurrent neural networks (RNNs) are also applied in large vocabulary continuous speech recognition (LVCSR) task, because LSTM networks have shown better performance than Fully-connected feed-forward deep neural network[2, 3, 4, 5].

Training neural network becomes more challenge when it goes deep. A conceptual tool called linear classifier probe is introduced to better understand the dynamics inside a neural network [6]. The discriminating features of linear classifier is the hidden units of a intermediate layer. For deep neural networks, it is observed that deeper layer's accuracy is lower than that of shallower layers. Therefore, the tool shows the difficulty of deep neural model training visually.

Layer-wise pre-training is a successful method to train very deep neural networks [7]. The convergence becomes harder with increasing the number of layers, even though the model is initialized with Xavier or its variants [8, 9]. But the deeper network which is initialized with a shallower trained network could converge well.

The size of LVCSR training dataset goes larger and training with only one GPU becomes high time consumption inevitably. Therefore, parallel training with multi-GPUs is more suitable for LVCSR system. Mini-batch based stochastic gradient descent (SGD) is the most popular method in neural network training procedure. Asynchronous SGD is a successful effort for parallel training based on it [10, 11]. It can many times speed up the training time without decreasing the accuracy. Besides, synchronous SGD is another effective effort, where the parameter server waits for every works to finish their computation and sent their local models to it, and then it sends updated model back to all workers [12]. Synchronous SGD converges well in parallel training with data parallelism, and is also easy to implement.

In order to further improve the performance of deep neural network with parallel training, several methods are proposed. Model averaging method achieves linear speedup, as the final model is averaged from all parameters of local models in different workers [13, 14], but the accuracy decreases compared with single GPU training. Moreover, blockwise model-updating filter (BMUF) provides another almost linear speedup approach with multi-GPUs on the basis of model averaging. It can achieve improvement or no-degradation of recognition performance compared with mini-batch SGD on single GPU [15].

Moving averaged (MA) approaches are also proposed for parallel training. It is demonstrated that the moving average of the parameters obtained by SGD performs as well as the parameters that minimize the empirical cost, and moving average parameters can be used as the estimator of them, if the size of training data is large enough [16]. One pass learning is then proposed, which is the combination of learning rate schedule and averaged SGD using moving average [17]. Exponential moving average (EMA) is proposed as a non-interference method[18]. EMA model is not broadcasted to

One-Shot Imitation Learning

Yan Duan [1 2] **Marcin Andrychowicz** [1] **Bradly C. Stadie** [1 2] **Jonathan Ho** [1 2] **Jonas Schneider** [1] **Ilya Sutskever** [1]
Pieter Abbeel [1 2] **Wojciech Zaremba** [1]

Abstract

Imitation learning has been commonly applied to solve different tasks in isolation. This usually requires either careful feature engineering, or a significant number of samples. This is far from what we desire: ideally, robots should be able to learn from very few demonstrations of any given task, and instantly generalize to new situations of the same task, without requiring task-specific engineering. In this paper, we propose a meta-learning framework for achieving such capability, which we call *one-shot imitation learning*.

Specifically, we consider the setting where there is a very large (maybe infinite) set of tasks, and each task has many instantiations. For example, a task could be to stack all blocks on a table into a single tower, another task could be to place all blocks on a table into two-block towers, etc. In each case, different instances of the task would consist of different sets of blocks with different initial states. At training time, our algorithm is presented with pairs of demonstrations for a subset of all tasks. A neural net is trained that takes as input one demonstration and the current state (which initially is the initial state of the other demonstration of the pair), and outputs an action with the goal that the resulting sequence of states and actions matches as closely as possible with the second demonstration. At test time, a demonstration of a single instance of a new task is presented, and the neural net is expected to perform well on new instances of this new task. Our experiments show that the use of soft attention allows the model to generalize to conditions and tasks unseen in the training data. We anticipate that by training this model on a much greater variety of tasks and settings, we will obtain a general system that can turn any demonstrations into robust policies that can accomplish an overwhelming variety of tasks.

[1]OpenAI [2]University of California, Berkeley. Correspondence to: Yan Duan <rocky@openai.com>.

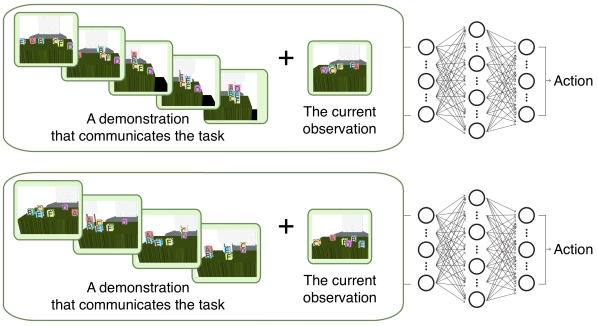

One-shot policy. A single policy trained to solve many tasks.

(left) Task-specific policy. This policy is trained to stack blocks into two towers, each of height 3. (right) A separate task-specific policy. This policy is trained to stack blocks into three towers, each of height 2.

Figure 1. Traditionally, policies are task-specific. For example, a policy might have been trained (through imitation or reinforcement learning) to stack blocks into towers of height 3, and then another policy would be trained to stack blocks into towers of height 2, etc. In this paper, we are interested in policies that are *not* specific to one task, but rather can be told (through a single demonstration) what the current new task is, and be successful at this new task. As illustrative examples, we would want to be able to provide a single demonstration of each task, and from that the one-shot policy would know what to do when faced with a new situation of the task, where the blocks are randomly rearranged. Videos of the illustrated tasks are available at `http://bit.ly/one-shot-imitation`.

1. Introduction

We are interested in robotic systems that are able to perform a variety of complex useful tasks, e.g. tidying up a home or preparing a meal. The robot should be able to learn new tasks without long system interaction time. To accomplish this, we must solve two broad problems:

- The first problem is that of dexterity: robots should learn how to approach, grasp and pick up complex un-

Deep brain fluorescence imaging with minimally invasive ultra-thin optical fibers

Shay Ohayon [1,2], Antonio M. Caravaca-Aguirre[3], Rafael Piestun[3], James J. DiCarlo[1,2]

(1) Mcgovern Institute for Brain Research, Massachusetts Institute of Technology, 43 Vassar Street Cambridge, MA 02139
(2) Department of Brain and Cognitive Sciences, Massachusetts Institute of Technology, 77 Massachusetts Avenue, Cambridge, MA 02139
(3) Department of Electrical, Computer, and Energy Engineering, University of Colorado, Boulder, Colorado, 80309, USA

Abstract

A major open challenge in neuroscience is the ability to measure and perturb neural activity in vivo from well-defined neural sub-populations at cellular resolution anywhere in the brain. However, limitations posed by scattering and absorption prohibit non-invasive (surface) multiphoton approaches[1,2] for deep (>2mm) structures, while Gradient Refreactive Index (GRIN) endoscopes[2–4] are thick and cause significant damage upon insertion. Here, we demonstrate a novel microendoscope to image neural activity at arbitrary depths via an ultrathin multimode optical fiber (MMF) probe that is 5-10X thinner than commercially available microendoscopes. We demonstrate micron-scale resolution, multispectral and volumetric imaging. In contrast to previous approaches[1,5–8] we show that this method has an improved acquisition speed that is sufficient to capture rapid neuronal dynamics in-vivo in rodents expressing a genetically encoded calcium indicator. Our results emphasize the potential of this technology in neuroscience applications and open up possibilities for cellular resolution imaging in previously unreachable brain regions.

1. Introduction

The main potential advantage of MMF for biological endoscopy is their thin diameter (50-150 um) which induces less damage compared to thicker probes, such as GRIN lens[4,9–11]. Fiber bending remains a major challenge to MMF imaging techniques that are based on Wavefront shaping (WFS) since fiber deformation changes how modes are coupled and invalidates precomputed transformations critical for image formation[12–14]. However, in some domains, such as neuroscience, major fiber bending may not always pose a direct problem since in many experimental designs fibers can be inserted into the brain along a straight trajectory to target specific brain regions. Furthermore, minor perturbations at the distal end of the fiber have only minor effects on the imaging capability if a proper fiber is selected[15]. Other challenges, on the other hand, need to be addressed to make this technology useful for neuroscience. First, acquisition speed needs to be sufficiently high to capture rapid neural firing events (ms scale), while maintaining sufficient spatial resolution to resolve cellular level details. Previous approaches[1,5–8] that use liquid crystal spatial light modulators (LC-SLM) have not been shown to be capable of this temporal resolution which would prohibit rapid sampling of neural signals. Second, the system needs to have high collection efficiency to capture small fluorescence changes evoked by calcium transients without causing photobleaching. To date, only fixed tissue has been successfully imaged[5,15]. Third, the system should image some distance away from the fiber tip since tissue in close proximity may not be functioning properly due to possible damage inflicted by fiber insertion.

Here, we focus on addressing these challenges and propose a novel microendoscope system that is based on a digital mirror device (DMD).

2. Methods

2.1 Generating phase modulation with a digital mirror device

The basic idea behind the Lee hologram[16] technique is to create a binary mask that creates a diffraction pattern with the desired phase modulation. Following the work of [16,17], to create a 2D spatial phase mask (x,y), we first define a spatial carrier wave with frequency f and rotation ,over the mirror domain [x,y]. The mask is then defined as:

$$X = \cos(\theta)\, x + \sin(\theta)\, y \tag{1}$$

$$Mask = \frac{1}{2}(1 + \cos\big(2\pi X - \Phi(x,y)\big) > 0.5 \tag{2}$$

This mask generates three peaks on the Fourier plane since

$$\frac{1}{2}(1 + \cos\big(2\pi X - \Phi(x,y)\big) = \frac{1}{2} + \frac{1}{4}e^{2\pi j(x-y)f_0}e^{-j\Phi(x,y)} + \frac{1}{4}e^{-2\pi j(x-y)f_0}e^{j\Phi(x,y)} \tag{3}$$

By blocking the first two terms (DC and one diffraction order) with an iris and allowing only one diffraction order to pass through, we create a 2D phase array that is up to a constant shift from the desired $\Phi(x,y)$.In the limit, each phase $\Phi(x,y)$ cannot be represented by a single mirror on the DMD, hence multiple mirrors are grouped to represent a single desired phase. We have experimented with varying sampling (number of mirrors per phase) and found that 10 is a good compromise between the size of each block and sufficient remaining mirrors to deliver the constant reference phase (see below).

2.2 Transmission matrix estimation and spot generation

On the Impossibility of Supersized Machines

Ben Garfinkel , Miles Brundage[1], Daniel Filan[2], Carrick Flynn[3], Jelena Luketina , Michael Page , Anders Sandberg[3], Andrew Snyder-Beattie[3], and Max Tegmark[4]

[1] *School for the Future of Innovation in Society, Arizona State University*
[2] *Department of Computer Science, University of California, Berkeley*
[3] *Future of Humanity Institute, University of Oxford*
[4] *Department of Physics, Massachusetts Institute of Technology*

April 1, 2017

Abstract

In recent years, a number of prominent computer scientists, along with academics in fields such as philosophy and physics, have lent credence to the notion that machines may one day become as large as humans. Many have further argued that machines could even come to exceed human size by a significant margin. However, there are at least seven distinct arguments that preclude this outcome. We show that it is not only implausible that machines will ever exceed human size, but in fact impossible.

Introduction

The history of life is often understood as a story of growth. If one takes the long view, then one can trace an exponential curve from our minuscule earliest ancestors, which were little more than self-replicating molecules, to the substantial creatures that we are today (Payne, 2009).

Although humanity became aware of this story only in the 19th century, through the work of Charles Darwin, we have long had the privilege of witnessing a partial recapitulation every time someone new comes into the world (Darwin, 1859). Before each person is a full-sized adult, they are first an invisibly small cell.

It is perhaps no surprise, then, that human largeness has for thousands of years fascinated many of our greatest thinkers. While some have sought to understand the nature and origins of largeness, others have anxiously inquired: *Could there ever be something larger than a human?*

Evidence of this anxiety can be found as far back as humanity's oldest recorded myth, *The Epic of Gilgamesh*, in which the monstrous giant Humbaba is appointed by Enlil, the king of the gods, to terrorize mankind (Sandars,

Associative content-addressable networks with exponentially many robust stable states

Rishidev Chaudhuri[1] and Ila Fiete[1]

[1]Center for Learning and Memory and Department of Neuroscience, The University of Texas at Austin, Austin, Texas, USA.

Abstract

The brain must robustly store a large number of memories, corresponding to the many events and scenes a person encounters over a lifetime. However, the number of memory states in existing neural network models either grows weakly with network size or recall performance fails catastrophically with vanishingly little noise. Here we show that it is possible to construct an associative content-addressable memory (ACAM) with *exponentially* many stable states and robust error-correction. The network possesses expander graph connectivity on a restricted Boltzmann machine architecture. The expansion property allows simple neural network dynamics to perform at par with modern error-correcting codes. Appropriate networks can be constructed with sparse random connections combined with glomerular nodes and a local associative learning rule, using low dynamic-range weights. Thus, sparse quasi-random constraint structures – characteristic of an important class of modern error-correcting codes – may provide for high-performance computation in artificial neural networks and the brain.

Introduction

Neural long-term memory systems have high capacity, by which we mean that the number of memory states is large. Such systems are also able to recover the correct memory state from partial or noisy cues, the definition of an associative memory. If the memory state can be addressed by its content, it is furthermore called content-addressable.

Classic studies of the dynamics and capacity of associative content-addressable neural memory (ACAM) have focused on connectionist neural network models commonly called Hopfield networks[1–3], which provide a powerful conceptual framework for thinking about pattern completion and associative memory in the brain. Here we continue in this tradition and examine constructions of ACAM networks in the form of Hopfield networks and their stochastic equivalents, Boltzmann machines. We show that it is possible to construct associative content-addressable memory networks with an unprecedented combination of robustness and capacity.

Mon. Not. R. Astron. Soc. **000**, 1–?? (2016) Printed 4 May 2017 (MN LATEX style file v2.2)

Transit Detection of a "Starshade" at the Inner Lagrange Point of an Exoplanet

E. Gaidos,[1⋆]
[1]*Department of Geology & Geophysics, University of Hawaii at Mānoa, Honolulu, Hawaii 96822 USA*

Submitted to MNRAS

ABSTRACT

All water-covered rocky planets in the inner habitable zones of solar-type stars will inevitably experience a catastrophic runaway climate due to increasing stellar luminosity and limits to outgoing infrared radiation from wet greenhouse atmospheres. Reflectors or scatterers placed near Earth's inner Lagrange point ($\mathcal{L}_1$) have been proposed as a "geo-engineering" solution to anthropogenic climate change and an advanced version of this could modulate incident irradiation over many Gyr or "rescue" a planet from the interior of the habitable zone. The distance of the starshade from the planet that minimizes its mass is 1.6 times the Earth-$\mathcal{L}_1$ distance. Such a starshade would have to be similar in size to the planet and the mutual occultations during planetary transits could produce a characteristic maximum at mid-transit in the light-curve. Because of a fortuitous ratio of densities, Earth-size planets around G dwarf stars present the best opportunity to detect such an artifact. The signal would be persistent and is potentially detectable by a future space photometry mission to characterize transiting planets. The signal could be distinguished from natural phenomenon, i.e. starspots or cometary dust clouds, by its shape, persistence, and transmission spectrum.

Key words: techniques: photometric – planets and satellites: terrestrial planets – astrobiology – extraterrestrial intelligence –

1 INTRODUCTION

Like every liquid water-covered planet around a solar-mass star, Earth has a serious greenhouse problem. As the Sun converts hydrogen to helium and becomes denser, hotter, and more luminous (Gough 1981) the inexorable increase in incident irradiation on Earth will, all else being equal, cause surface temperatures to rise and the atmosphere to contain more water vapor. Water is an efficient greenhouse gas, creating a positive feedback in Earth's climate system as more water vapor leads to elevated temperatures, and vice verse. Walker, Hays & Kasting (1981) proposed that temperature-dependent aqueous weathering and precipitation of carbonate minerals acts as a negative climate feedback that adjusts atmospheric CO_2 to maintain weathering at a rate that balances volcanic degassing, i.e. surface temperatures permissive of abundant liquid water.

However this planetary "thermostat" has its limits. As irradiance continues to increase, CO_2 will eventually disappears from the atmosphere causing a crisis for land plant life and any indeed any autotrophic life relying on atmospheric CO_2 as a source of carbon (Caldeira & Kasting 1992). Beyond this point, increasing irradiance cannot be compensated by diminished CO_2 and temperatures rise. Climate models predict an asymptotic (maximum) value for the outgoing infrared radiation of an Earth-like atmosphere as a function of temperature; if the absorbed incident radiation exceeds this value, temperatures will increase until the oceans evaporate (Ingersoll 1969). At that point multiple "runaway" climate feed-backs, not mutually exclusive, can occur: water vapor in the upper atmosphere will be photolyzed and the escape of hydrogen will lead to loss of water. Continued de-gassing of CO_2 from the mantle will not be compensated by aqueous weathering of silicates and formation of carbonates, enhancing the greenhouse effect and causing higher surface temperatures. Eventually, surface temperatures will exceed the stability of carbonate minerals, leading to the breakdown of carbonate rocks in the crust, the release of ≈90 bars of CO_2 into the atmosphere (Tuck 1980), a Venus-like climate, and the complete extinction of the biosphere. Because of stellar luminosity evolution, all Earth-like planets within the "conservative" habitable zone of solar-mass stars (0.95-1.67 AU Kopparapu et al. 2013) will eventually orbit interior to the habitable zone and meet this fate.

⋆ Visiting Scientist, Center for Space and Habitability, University of Bern, Bern, Sitzerland. E-mail: gaidos@hawaii.edu (EG)

Improving Nanopore Reads Raw Signal Alignment

Vladimír Boža, Broňa Brejová, and Tomáš Vinař

Faculty of Mathematics, Physics, and Informatics, Comenius University,
Mlynská dolina, 842 48 Bratislava, Slovakia
{boza,brejova,vinar}@fmph.uniba.sk

Abstract. We investigate usage of dynamic time warping (DTW) algorithm for aligning raw signal data from MinION sequencer. DTW is mostly using for fast alignment for selective sequencing to quickly determine whether a read comes from sequence of interest.
We show that standard usage of DTW has low discriminative power mainly due to problem with accurate estimation of scaling parameters. We propose a simple variation of DTW algorithm, which does not suffer from scaling problems and has much higher discriminative power.

1 Introduction

In this paper, we propose improvements to algorithms for aligning raw signals from MinION nanopore sequencer. The MinION device by Oxford Nanopore (Mikheyev and Tin, 2014), weighing only 90 grams, is currently the smallest high-throughput DNA sequencer. Thanks to its low capital costs, small size and the possibility of analyzing the data in real time as they are produced, MinION is very promising for clinical applications, such as monitoring infectious disease outbreaks (Quick et al., 2015, 2016), and characterizing structural variants in cancer (Norris et al., 2016).

One of the MinION advantages is selective sequencing, where we only sequence "interesting" reads by rejecting all other reads after reading the first few hundred bases. The idea was mostly explored in Readuntil tool (Loose et al., 2016).

Hard part of selective sequencing is deciding which reads to reject. Standard algorithm for selective sequencing would be to base call the first few hundreds of events from the read and then align them to the reference sequence. After aligning, we would accept the read if we find a match with the acceptable similarity.

Unfortunately, the speed of the base calling algorithm on a reasonable computer is much lower than the rate at which the sequencer produces the data. This means that we need to use other approaches than base calling followed by alignment. We will explore an approach which does not translate electric signal into DNA, but instead it works directly with the electric signal data.

Loose et al. (2016) solved this problem using dynamic time warping algorithm (DTW), but he only align reads to small target sequences with size up to hundred kilobases.

Morphological Error Detection in 3D Segmentations

David Rolnick[1]*, **Yaron Meirovitch**[1], **Toufiq Parag**[2], **Hanspeter Pfister**[2]
Viren Jain[3], **Jeff W. Lichtman**[2], **Edward S. Boyden**[1], **Nir Shavit**[1]
[1]Massachusetts Institute of Technology, [2]Harvard University, [3]Google, Inc.

Abstract

Deep learning algorithms for connectomics rely upon localized classification, rather than overall morphology. This leads to a high incidence of erroneously merged objects. Humans, by contrast, can easily detect such errors by acquiring intuition for the correct morphology of objects. Biological neurons have complicated and variable shapes, which are challenging to learn, and merge errors take a multitude of different forms. We present an algorithm, MergeNet, that shows 3D ConvNets can, in fact, detect merge errors from high-level neuronal morphology. MergeNet follows unsupervised training and operates across datasets. We demonstrate the performance of MergeNet both on a variety of connectomics data and on a dataset created from merged MNIST images.

1 Introduction

The neural network of the brain remains a mystery, even as engineers have succeeded in building artificial neural networks that can solve a wide variety of problems. Understanding the brain at a deeper level could significantly impact both biology and artificial intelligence [3, 8, 19, 23, 35]. Perhaps appropriately, artificial neural networks are now being used to map biological neural networks. However, humans still outperform computer vision algorithms in segmenting brain tissue. Deep learning has not yet attained the intuition that allows humans to recognize and trace the fine, intermingled branches of neurons.

The field of *connectomics* aims to reconstruct three-dimensional networks of biological neurons from high-resolution microscope images. Automated segmentation is a necessity due to the quantities of data involved. In one recent study [9], the brain of a larval zebrafish was annotated by hand, requiring more than a year of human labor. It is estimated that mapping a single human brain would require a zettabyte (one billion terabytes) of image data [17], clearly more than can be manually segmented.

State-of-the-art algorithms apply a convolutional neural network (ConvNet) to predict, for each voxel of an image, whether it is on the boundary (*cell membrane*) of a neuron. The predicted membranes are then filled in by subsequent algorithms [10]. Such methods are prone both to *split errors*, in which true objects are subdivided, and to *merge errors*, in which objects are fused together. The latter pose a particular challenge. Neurons are highly variable, unpredictably sprouting thousands of branches, so their correct shapes cannot be catalogued. Erroneously merged neurons are obvious to trained humans because they simply don't look right, but it has hitherto been impossible to make such determinations automatically.

*Correspondence should be addressed to: drolnick@mit.edu.

Genuine Multipartite Entanglement in the 3-Photon Decay of Positronium

Beatrix C. Hiesmayr[1] and Pawel Moskal[2]

[1]*Faculty of Physics, University of Vienna, Boltzmanngasse 5, 1090 Vienna, Austria*
[2]*Institute of Physics, Jagiellonian University, Cracow, Poland*

The electron-positron annihilation into two photons is a standard technology in medicine to observe e.g. metabolic processes in human bodies. A new tomograph will provide the possibility to observe not only direct e^+e^- annihilations but also the 3 photons from the decay of ortho-positronium atoms formed in the body. We show in this contribution that the three-photon state with respect to polarisation degrees of freedom depends on the angles between the photons and exhibits various specific entanglement features. In particular genuine multipartite entanglement, a type of entanglement involving all degrees of freedoms, is subsistent if the positronium was in a definite spin eigenstate. Remarkably, when all spin eigenstates are mixed equally, entanglement – and even stronger genuine multipartite entanglement– survives. Due to a "*symmetrization*" process, however, *Dicke*-type of entanglement remains whereas GHZ-type of entanglement vanishes. The survival of particular entanglement properties in the mixing scenario may make it possible to extract quantum information in form of distinct entanglement features, e.g., from metabolic processes in human bodies.

I. INTRODUCTION

The detection of the two high energetic photons coming from the annihilation of an electron and a positron is a well-established successful technology to image metabolic processes in living bodies (PET: Positron Emission Tomography). PET application are used in many different fields of medicine, e.g. in oncology, in cardiology, in radiation therapy or in neurology. In recent years, PET instrumentation has undergone a steady multifaceted evolution and the improvements include new hardware, new reconstruction methods and implementation of time-of-flight techniques [1–7].

With no doubt PET serves as an important tool in imaging metabolic processes based on the sensitivity to tracers (positron-emitting radionuclides) injected into the body or tissue.

Electron-positron annihilations may occur either directly or via the creation of positronium atoms (a bound state of electron and positron). Positronium [8–11] can be in an anti-symmetric spin state (para-positronium) or a symmetric spin state (ortho-positronium). Charge conjugation implies that in the first case it decays into an even number of photons (2γ, 4γ,...) and in the other case into an odd number of photons (3γ, 5γ,...). Due to kinematics and smallness of the fine-structure constant the 2γ and 3γ cases are the two most likely options. Since positronium atoms are formed copiously inside the human body during routine PET imaging 3γ-decays occur also frequently. Even in water the production of ortho-positronium has a probability equal to about 25% [12] and is expected to be more than 38% in a tissue [13]. Three-photon events, however, have never been used in tomography because of technical limitations of standard PET devices. A new prototype, called J-PET (Jagiellonian-PET) [14–19], has shown to meet all technical requirements in performing such a measurement for the first time.

This paper investigates the entanglement in the polarisation degrees of freedom of the three photons resulting from the decay of the ortho-positronium. Both for a fixed spin quantization direction of the positronium as well as the case of equal mixing. Photons are fascinating quantum systems, having spin one, but due to their massless property there is a nontrivial coupling between the spin and momentum properties. The most appropriate single-photon description remains controversial. A recent framework describing all single-photon states and single-photon observables by POVMs (positive-operator valued measurements) can be found in Ref. [20]. In this contribution we restrict ourselves to the polarisation degrees of freedom and are interested in the correlation of three photons with energies that ranges from 0 to 511keV. Entanglement and in particular multipartite entanglement is a highly investigated field that has the potential to become a new technology. This paper makes a step towards investigating what type of entanglement is present in the three-photon state generated by the decay of ortho-positronium. This may one day result in obtaining not only the local information where in a tissue the positronium decays, but as well revealing the quantum information which may serve as a new quantum marker for specific biological processes.

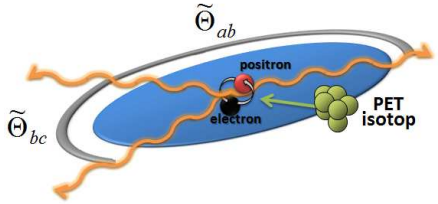

FIG. 1: (Color online) This graphic shows schematically how from an isotop typically used in standard PET-therapy, e.g. FDG-18 (fludeoxyglucose), positronium is generated that decays into three photons which wave vectors have to lay in one plane due to energy and momentum conservation.

Note that entanglement seems to play an important

Quantum Resource Estimates for Computing Elliptic Curve Discrete Logarithms

Martin Roetteler, Michael Naehrig, Krysta M. Svore, and Kristin Lauter

Microsoft Research, USA

Abstract. We give precise quantum resource estimates for Shor's algorithm to compute discrete logarithms on elliptic curves over prime fields. The estimates are derived from a simulation of a Toffoli gate network for controlled elliptic curve point addition, implemented within the framework of the quantum computing software tool suite LIQ$Ui|\rangle$. We determine circuit implementations for reversible modular arithmetic, including modular addition, multiplication and inversion, as well as reversible elliptic curve point addition. We conclude that elliptic curve discrete logarithms on an elliptic curve defined over an n-bit prime field can be computed on a quantum computer with at most $9n + 2\lceil \log_2(n) \rceil + 10$ qubits using a quantum circuit of at most $448n^3 \log_2(n) + 4090n^3$ Toffoli gates. We are able to classically simulate the Toffoli networks corresponding to the controlled elliptic curve point addition as the core piece of Shor's algorithm for the NIST standard curves P-192, P-224, P-256, P-384 and P-521. Our approach allows gate-level comparisons to recent resource estimates for Shor's factoring algorithm. The results also support estimates given earlier by Proos and Zalka and indicate that, for current parameters at comparable classical security levels, the number of qubits required to tackle elliptic curves is less than for attacking RSA, suggesting that indeed ECC is an easier target than RSA.

Keywords: Quantum cryptanalysis, elliptic curve cryptography, elliptic curve discrete logarithm problem.

1 Introduction

Elliptic curve cryptography (ECC). Elliptic curves are a fundamental building block of today's cryptographic landscape. Thirty years after their introduction to cryptography [31,27], they are used to instantiate public key mechanisms such as key exchange [11] and digital signatures [17,23] that are widely deployed in various cryptographic systems. Elliptic curves are used in applications such as transport layer security [10,5], secure shell [46], the Bitcoin digital currency system [33], in national ID cards [22], the Tor anonymity network [12], and the WhatsApp messaging app [52], just to name a few. Hence, they play a significant role in securing our data and communications.

Different standards (e.g., [8,49]) and standardization efforts (e.g., [13,35]) have identified elliptic curves of different sizes targeting different levels of security. Notable curves with widespread use are the NIST curves P-256, P-384, P-521, which are curves in Weierstrass form over special primes of size 256, 384, and 521 bits respectively, the Bitcoin curve `secp256k1` from the SEC2 [8] standard and the Brainpool curves [13]. More recently, Bernstein's Curve25519 [53], a Montgomery curve over a 255-bit prime field, has seen more and more deployment, and it has been recommended to be used in the next version of the TLS protocol [29] along with another even more recent curve proposed by Hamburg called Goldilocks [20].

The security of elliptic curve cryptography relies on the hardness of computing discrete logarithms in elliptic curve groups, i.e. the difficulty of the Elliptic Curve Discrete Logarithm Problem (ECDLP). Elliptic curves have the advantage of relatively small parameter and key sizes in comparison to other cryptographic schemes, such as those based on RSA [40] or finite field discrete logarithms [11], when compared at the same security level. For example, according to NIST recommendations from 2016, a 256-bit elliptic curve provides a similar resistance against classical

Learning Macromanagement in StarCraft from Replays using Deep Learning

Niels Justesen
IT University of Copenhagen
Copenhagen, Denmark
noju@itu.dk

Sebastian Risi
IT University of Copenhagen
Copenhagen, Denmark
sebr@itu.dk

***Abstract*—The real-time strategy game StarCraft has proven to be a challenging environment for artificial intelligence techniques, and as a result, current state-of-the-art solutions consist of numerous hand-crafted modules. In this paper, we show how macromanagement decisions in StarCraft can be learned directly from game replays using deep learning. Neural networks are trained on 789,571 state-action pairs extracted from 2,005 replays of highly skilled players, achieving top-1 and top-3 error rates of 54.6% and 22.9% in predicting the next build action. By integrating the trained network into UAlbertaBot, an open source StarCraft bot, the system can significantly outperform the game's built-in Terran bot, and play competitively against UAlbertaBot with a fixed rush strategy. To our knowledge, this is the first time macromanagement tasks are learned directly from replays in StarCraft. While the best hand-crafted strategies are still the state-of-the-art, the deep network approach is able to express a wide range of different strategies and thus improving the network's performance further with deep reinforcement learning is an immediately promising avenue for future research. Ultimately this approach could lead to strong StarCraft bots that are less reliant on hard-coded strategies.**

I. Introduction

Artificial neural networks have been a promising tool in machine learning for many tasks. In the last decade, the increase in computational resources as well as several algorithmic improvements, have allowed deep neural networks with many layers to be trained on large datasets. This approach, also re-branded as *deep learning*, has remarkably pushed the limits within object recognition [13], speech recognition [8], and many other domains. Combined with reinforcement learning, these techniques have surpassed the previous state-of-the-art in playing Atari games [16], the classic board game Go [23] and the 3D first-person shooter Doom [15].

An open challenge for these methods are real-time strategy (RTS) games such as StarCraft, which are highly complex on many levels because of their enormous state and actions space with a large number of units that must be controlled in real-time. Furthermore, in contrast to games like Go, AI algorithms in StarCraft must deal with hidden information; the opponent's base is initially hidden and must be explored continuously throughout the game to know (or guess) what strategy the opponent is following. The game has been a popular environment for game AI researchers with several StarCraft AI competitions such as the *AIIDE StarCraft AI Competition*[1], *CIG StarCraft RTS AI Competition*[2] and the *Student StarCraft AI Competition*[3].

However, bots participating in these competitions rely mainly on hard-coded strategies [6, 20] and are rarely able to adapt to the opponent during the game. They usually have a modular control architecture that divides the game into smaller task areas, relying heavily on hand-crafted modules and developer domain knowledge. Learning to play the entire game with end-to-end deep learning, as it was done for Atari games [16], is currently an unsolved challenge and perhaps an infeasible approach. A simpler approach, which we follow in this paper, is to apply deep learning to replace a specific function in a larger AI architecture.

More specifically, we focus on applying deep learning to macromanagement tasks in *StarCraft: Brood War* in the context of deciding what to produce next. A neural network is trained to predict these decisions based on a training set extracted from replay files (i.e. game logs) of highly skilled human players. The trained neural network is combined with the existing StarCraft bot UAlbertaBot, and is responsible for deciding what unit, building, technology, or upgrade to produce next, given the current state of the game. While our approach does not achieve state-of-the-art results on its own, it is a promising first step towards self-learning methods for macromanagement in RTS games. Additionally, the approach presented here is not restricted to StarCraft and can be directly applied to other RTS games as well.

II. StarCraft

StarCraft is a real-time strategy (RTS) game released by Blizzard in 1998. The same year an expansion set called *StarCraft: Brood War* was released, which became so popular that a professional StarCraft gamer scene emerged. The game is a strategic military combat simulation in a science fiction setting. Each player controls one of three races; Terran, Protoss and Zerg. During the game, they must gather resources to expand their base and produce an army. The winner of a game is the player that manages to destroy the opponent's base. Figure 1 shows a screenshot from a player's perspective controlling the Protoss. The screenshot shows numerous workers

[1] http://www.cs.mun.ca/~dchurchill/starcraftaicomp/
[2] http://cilab.sejong.ac.kr/sc_competition/
[3] http://sscaitournament.com/

Centimeter-Scale Suspended Photonic Crystal Mirrors

João P. Moura,[1,*] Richard A. Norte,[1,†,*] Jingkun Guo,[1] Clemens Schäfermeier,[1] and Simon Gröblacher[1,‡]

[1] *Kavli Institute of Nanoscience, Delft University of Technology, Lorentzweg 1, 2628CJ Delft, The Netherlands*

Demand for lightweight, highly reflective and mechanically compliant mirrors for optics experiments has recently seen a significant surge. Due to their bulky geometry, standard mirror solutions have a high mass, which severely limits their use in applications such as light sails [1], evanescent field sensors [2, 3], or deformable mirrors [4]. Advances in nanofabrication have shown that photonic crystal (PhC) membranes [5] are an ideal alternative to conventional mirrors, as they provide high reflectivity with only a single layer of dielectric material. In particular, devices made of silicon nitride constitute the state-of-the-art in PhC mirrors with low optical absorption and mechanical loss [6–8]. However, fabrication technology has constrained their effective area to a few square-micrometers. Here we experimentally demonstrate the first example of suspended PhC mirrors spanning areas up to $10 \times 10\,\mathrm{mm}^2$. We overcome the limitations imposed by the finite size of the PhC, which allows us to measure reflectivities greater than 99 % on 210 nm thin devices at 1550 nm wavelength and beyond 90 % on 56 nm thick mirrors – an unrivaled performance compared to PhC mirrors with micro scale diameters. We also consider their use as mirrors in gravitational wave detectors where they could potentially reduce mirror coating noise at cryogenic temperatures. These structures bridge the gap between nano scale technologies and macroscopic optical elements.

Photonic crystal (PhC) membranes are suspended dielectric sheets patterned with sub-wavelength, low-index two-dimensional periodic structures [5]. These patterns give rise to resonances that can couple out-of-plane radiation to in-plane guided modes, and can be engineered to transform a flat membrane into a mirror [9], a lens [10], or even a curved mirror [10–12]. Here we study a PhC consisting of a periodic lattice of holes in a membrane, whose hole radius and lattice constant can be tuned to reflect light at a wavelength of choice. When fabricated from materials with low optical absorption such as low-pressure chemically vapor-deposited silicon nitride (LPCVD SiN), one can realize mirrors with sub-wavelength thicknesses and reflectivities $> 99\,\%$, only limited by scattering losses [8]. LPCVD SiN thin films also enable the combination of PhC mirrors with low thermal noise mechanical oscillators, due to their high intrinsic stress, thin geometry, and weak coupling to undesired thermal modes [6, 13].

Limitations in microfabrication processes have so far restricted suspended PhC mirrors to areas not much bigger than $100 \times 100\,\mu\mathrm{m}^2$. This size sets an upper bound to the waist of incident Gaussian beams, since wider waists do not completely interact with the PhC, resulting in decreased reflectivity. But the beams also have a lower bound, since very small waists have a high divergence and couple to undesired PhC modes, which leads to shifting, broadening and shallowing of the reflectivity. These adverse finite-size effects have been consistently measured in very thin mirrors with thicknesses below 0.1λ, where λ is the wavelength of the reflected light [6, 7, 14, 15]. The ability to fabricate larger PhC mirrors with increasingly thinner membranes could greatly facilitate the combination of high reflectivity and low mechanical clamping losses [6]. These properties are crucial for reducing thermal mirror coating noise which stands as a limit in precision measurements such as atomic clocks [16], frequency-stabilized lasers [17], and gravitational wave detectors [18]. At the centimeter scale, PhC mirrors could have more immediate applications as deformable mirrors with adjustable wavefront [4], or evanescent field sensors with a large interaction area [2, 3].

Scaling up suspended PhC mirrors even further to meter scales would make this technology compatible with a number of next-generation experiments. Some of the most promising avenues for interstellar exploration, for example, rely on the development of low-mass light sails (i.e. lightweight reflectors), which could be accelerated to 1/5 the speed of light using radiation pressure [1]. Initiatives like the Starshot Breakthrough [19] require meter-sized light sails with a thickness of only tens of nanometers – an aspect-ratio that is far beyond current nanotechnology and that stands out as one of the most daunting challenges of this ambitious project.

In this letter we experimentally demonstrate free-standing SiN photonic crystal mirrors with thicknesses of 56 and 210 nm and diameters of up to 10 mm. Not only do we increase the area of suspended PhC mirrors by nearly 4 orders of magnitude compared to previous works, we also show that these large aspect-ratios allow us to achieve high reflectivity from membranes 3 times thinner than previously measured. We observe greater than 90 % reflectivity of 1550 nm light from mirrors with a thickness of 0.038λ (56 nm) – an experimental first as PhC mirrors have consistently been limited to thicknesses above 0.13λ (210 nm at 1550 nm) to attain high reflectivity [6]. Such large structures allow studying the spec-

* These authors contributed equally to this work.
† r.a.norte@tudelft.nl
‡ s.groeblacher@tudelft.nl

Photographic Image Synthesis with Cascaded Refinement Networks

Qifeng Chen[†‡] Vladlen Koltun[†]

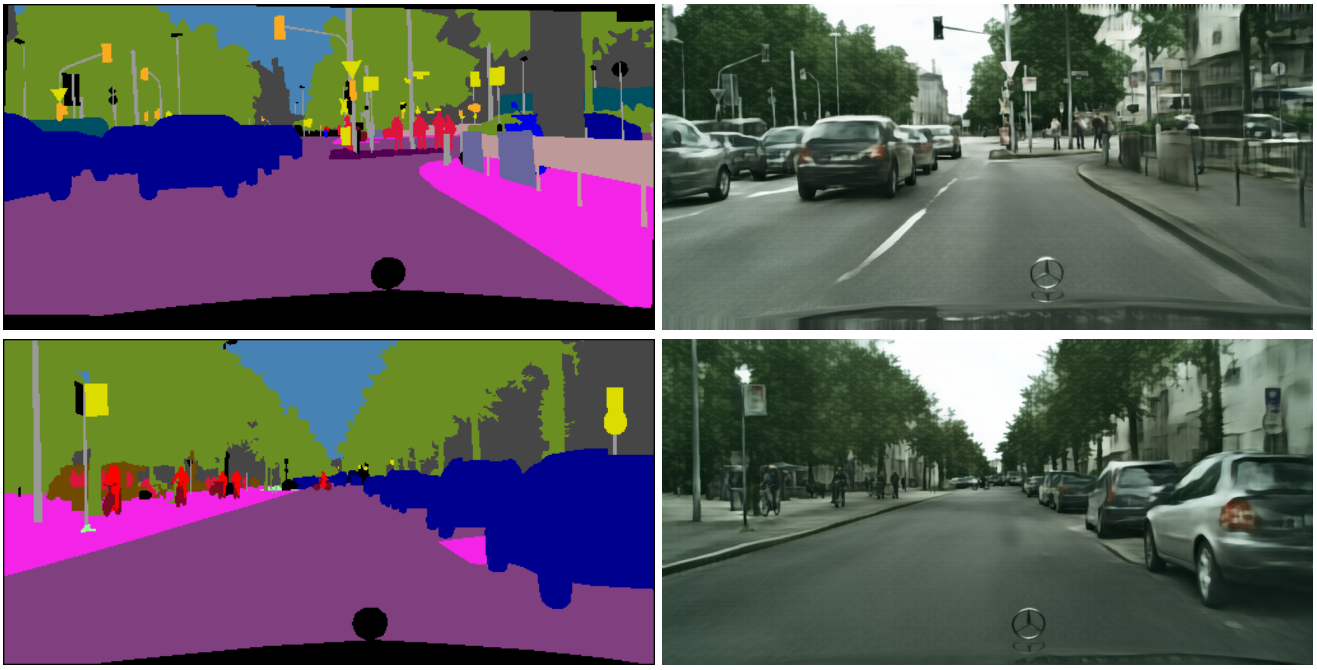

(a) Input semantic layouts (b) Synthesized images

Figure 1. Given a pixelwise semantic layout, the presented model synthesizes an image that conforms to this layout. (a) Semantic layouts from the Cityscapes dataset of urban scenes; semantic classes are coded by color. (b) Images synthesized by our model for these layouts. The layouts shown here and throughout the paper are from the validation set and depict scenes from new cities that were never seen during training. Best viewed on the screen.

Abstract

We present an approach to synthesizing photographic images conditioned on semantic layouts. Given a semantic label map, our approach produces an image with photographic appearance that conforms to the input layout. The approach thus functions as a rendering engine that takes a two-dimensional semantic specification of the scene and produces a corresponding photographic image. Unlike recent and contemporaneous work, our approach does not rely on adversarial training. We show that photographic images can be synthesized from semantic layouts by a single feedforward network with appropriate structure, trained end-to-end with a direct regression objective. The presented approach scales seamlessly to high resolutions; we demonstrate this by synthesizing photographic images at 2-megapixel resolution, the full resolution of our training data. Extensive perceptual experiments on datasets of outdoor and indoor scenes demonstrate that images synthesized by the presented approach are considerably more realistic than alternative approaches.

1. Introduction

Consider the semantic layouts in Figure 1. A skilled painter could draw images that depict urban scenes that conform to these layouts. Highly trained craftsmen can even create paintings that approach photorealism [20]. Can we train computational models that have this ability? Given a semantic layout of a novel scene, can an artificial system synthesize an image that depicts this scene and looks like a photograph?

[†]Intel Labs
[‡]Stanford University

Natural Language Processing with Small Feed-Forward Networks

Jan A. Botha **Emily Pitler** **Ji Ma** **Anton Bakalov**
Alex Salcianu **David Weiss** **Ryan McDonald** **Slav Petrov**
Google Inc.
Mountain View, CA
{jabot,epitler,maji,abakalov,salcianu,djweiss,ryanmcd,slav}@google.com

Abstract

We show that small and shallow feed-forward neural networks can achieve near state-of-the-art results on a range of unstructured and structured language processing tasks while being considerably cheaper in memory and computational requirements than deep recurrent models. Motivated by resource-constrained environments like mobile phones, we showcase simple techniques for obtaining such small neural network models, and investigate different tradeoffs when deciding how to allocate a small memory budget.

1 Introduction

Deep and recurrent neural networks with large network capacity have become increasingly accurate for challenging language processing tasks. For example, machine translation models have been able to attain impressive accuracies, with models that use hundreds of millions (Bahdanau et al., 2014; Wu et al., 2016) or billions (Shazeer et al., 2017) of parameters. These models, however, may not be feasible in all computational settings. In particular, models running on mobile devices are often constrained in terms of memory and computation.

Long Short-Term Memory (LSTM) models (Hochreiter and Schmidhuber, 1997) have achieved good results with small memory footprints by using character-based input representations: e.g., the part-of-speech tagging models of Gillick et al. (2016) have only roughly 900,000 parameters. Latency, however, can still be an issue with LSTMs, due to the large number of matrix multiplications they require (eight per LSTM cell): Kim and Rush (2016) report speeds of only 8.8 words/second when running a two-layer LSTM translation system on an Android phone.

Feed-forward neural networks have the potential to be much faster. In this paper, we show that small feed-forward networks can achieve results at or near the state-of-the-art on a variety of natural language processing tasks, with an order of magnitude speedup over an LSTM-based approach.

We begin by introducing the network model structure and the character-based representations we use throughout all tasks (§2). The four tasks that we address are: language identification (Lang-ID), part-of-speech (POS) tagging, word segmentation, and preordering for translation. In order to use feed-forward networks for structured prediction tasks, we use transition systems (Titov and Henderson, 2007, 2010) with feature embeddings as proposed by Chen and Manning (2014), and introduce two novel transition systems for the last two tasks. We focus on *budgeted* models and ablate four techniques (one on each task) for improving accuracy for a given memory budget:

1. Quantization: Using more dimensions and less precision (Lang-ID: §3.1).
2. Word clusters: Reducing the network size to allow for word clusters and derived features (POS tagging: §3.2).
3. Selected features: Adding explicit feature conjunctions (segmentation: §3.3).
4. Pipelines: Introducing another task in a pipeline and allocating parameters to the auxiliary task instead (preordering: §3.4).

We achieve results at or near state-of-the-art with small (< 3 MB) models on all four tasks.

2 Small Feed-Forward Network Models

The network architectures are designed to limit the memory and runtime of the model. Figure 1 illustrates the model architecture:

STARDATA: A StarCraft AI Research Dataset

Zeming Lin
Facebook
770 Broadway
New York, NY, 10003

Jonas Gehring
Facebook
6, rue Ménars
75002 Paris, France

Vasil Khalidov
Facebook
6, rue Ménars
75002 Paris, France

Gabriel Synnaeve
Facebook
770 Broadway
New York, NY, 10003

Abstract

We release a dataset of 65646 StarCraft replays that contains 1535 million frames and 496 million player actions. We provide full game state data along with the original replays that can be viewed in StarCraft. The game state data was recorded every 3 frames which ensures suitability for a wide variety of machine learning tasks such as strategy classification, inverse reinforcement learning, imitation learning, forward modeling, partial information extraction, and others. We use TorchCraft to extract and store the data, which standardizes the data format for both reading from replays and reading directly from the game. Furthermore, the data can be used on different operating systems and platforms. The dataset contains valid, non-corrupted replays only and its quality and diversity was ensured by a number of heuristics. We illustrate the diversity of the data with various statistics and provide examples of tasks that benefit from the dataset. We make the dataset available at https://github.com/TorchCraft/StarData. En Taro Adun!

Introduction

Real time strategy games as an AI research problem is attracting substantial attention (Ontañón et al. 2013; Usunier et al. 2016; Peng et al. 2017) due to their complex game dynamics, partial observability, and existing expert games in the form of human replays. These games are a good test bed for various reinforcement learning algorithms on a domain with higher complexity than toy robotics tasks and turn-based board games. Due to recent advances in deep learning, we see a trend of improved model performance with larger datasets. As learning capacity of these models increases, there is a growing need for data, especially in order to apply deep learning methods to control in RTS games.

Although learning in StarCraft can be performed through playing, the dynamics of the game are extremely complex, and it is beneficial to speed up learning by using existing games. The availability of datasets of recorded games between experienced players is therefore desirable.

StarCraft allows one to record replays of games which contain all commands issued by players. A number of online resources contain collections of replays from various tournaments (see Table 1). Some information can be directly inferred from the replay file; however, reconstructing the full game state requires playback in StarCraft.

There are several aspects that make it difficult to use the replays directly for machine learning purposes. *Firstly*, the reconstruction speed of StarCraft is limited and would impose an upper threshold on training speed. *Secondly*, incompatibility between replays produced by different StarCraft versions makes it impossible to use the same game engine for all the replays or might result in corrupted data. *Finally*, the reconstruction process can only be reliably run on Windows, which adds additional unnecessary restrictions. Hence, the utility of a replay dataset can be increased by extracting game states, validating them and storing them as a separate dataset.

For a dataset to serve as a good base for learning models, it should fulfill a number of requirements:

Universality: the data stored in the dataset can be used to learn different aspects of game strategy and at different levels. Thus the dataset should provide data which is not specific to any particular context and should be as close to the full game state as possible.

Diversity: the dataset should cover a variety of game scenarios in terms of match-ups, maps, player strategies, etc.

Validity: the dataset should be representative of the distribution of StarCraft matches where both sides are trying to win.

Interfacing: one should be able to easily substitute game states received from the game engine with game states recorded in the dataset.

Portability: dataset access should be supported on a variety of platforms and operating systems.

With these requirements in mind, we constructed a new dataset of StarCraft replays from games among humans that can be used for StarCraft AI research. The following are our major contributions.

We provide a large set of StarCraft human replays, which is about 10x bigger than any of the comparable datasets currently available. The dataset includes a variety of scenarios and thus ensures the *diversity* requirement. Detailed statistics on matchups, maps etc. can be found in further sections.

All replays are checked for playability in StarCraft and BWAPI. We used additional scripted rule-based checks for

DeepRebirth: Accelerating Deep Neural Network Execution on Mobile Devices

Dawei Li
Samsung Research America
dawei.l@samsung.com

Xiaolong Wang
Samsung Research America
xiaolong.w@samsung.com

Deguang Kong
doogkong@gmail.com

Abstract

Deploying deep neural networks on mobile devices is a challenging task due to computation complexity and memory intensity. Current model reduction methods (e.g., matrix approximation using SVD) cannot satisfy real-time processing requirement. This paper first discovers that the major obstacle is the excessive execution time of non-tensor layers (with tensor-like parameters) such as pooling and normalization. This motivates us to design a novel acceleration framework: DeepRebirth through "slimming" existing consecutive and parallel non-tensor and tensor layers. The layer slimming is executed at different substructures: (a) streamline slimming by merging the consecutive non-tensor and tensor layer vertically; (b) branch slimming by merging non-tensor and tensor branches horizontally. These different optimization operations accelerate the model execution and reduce the run-time memory cost significantly. To maximally avoid accuracy loss, the parameters in new generated layers are learned with layer-wise fine-tuning based on both theoretical analysis and empirical verification. As observed in the experiment, DeepRebirth achieves 3x-5x speed-up and energy saving on GoogLeNet with only 0.4% accuracy drop on top-5 categorization in ImageNet. Further, by combining with other model compression techniques, DeepRebirth offers an average of $65ms$ *model forwarding time on a single image using Samsung Galaxy S6 with 86.54% top-5 accuracy with 2.5x run-time memory saving.*

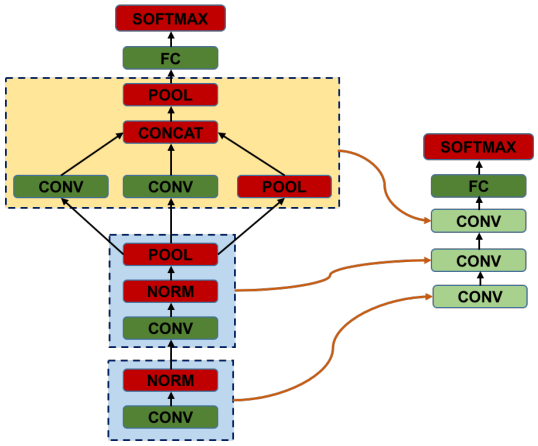

Figure 1: An illustration of proposed DeepRebirth model acceleration pipeline. DeepRebirth optimizes a trained deep learning model (left) to an accelerated "slim" model (right). Such optimization is achieved with two operations: Streamline Slimming which absorbs non-tensor layers (i.e., pooling and normalization) to their bottom convolutional layer (in light blue background) and Branch Slimming which absorbs non-tensor branches and convolutional branches with small convolution filters (e.g., 1x1) to a convolutional branch with large convolution filter (e.g., 5x5) (in light yellow background). We name new generated layers as slim layers.

1. Introduction

Recent years have witnessed the breakthrough of deep learning techniques for many computer vision tasks such as image classification and object detection. More and more mobile applications adopt deep learning techniques to provide accurate, intelligent and effective services. However, the execution speed of deep learning models on mobile devices becomes a bottleneck for deployment of many applications due to limited computing resources.

In this paper, we focus on improving the execution efficiency of deep learning models on mobile CPUs, which is a highly intriguing feature. On one hand, a large majority of mobile devices are equipped with mobile GPUs, however, the speed-up achieved is quite limited when compared to CPU [18], not to mention the complexity caused by different mobile GPU architectures. On the other hand, major deep learning frameworks such as Caffe [14] and Tensorflow [1] only support CPU implementation on mobile devices currently, and therefore an efficient CPU-friendly model is highly desirable. In reality, it takes more than 651ms to recognize an image using GoogleNet on Samsung S5 (Table 4) with 984mJ energy costs (Table 5). The effective solution is expected to provide minimum accuracy loss by leveraging widely used deep learning framework (such as GoogLeNet and ResNet) with support of deep model acceleration on different types of layers.

Visions of Human Futures in Space and SETI

Jason T. Wright

Department of Astronomy & Astrophysics and
Center for Exoplanets and Habitable Worlds
525 Davey Laboratory, The Pennsylvania State University,
University Park, PA, 16802, USA, astrowright@gmail.com

Visiting Associate Professor, Department of Astronomy
Breakthrough Listen Laboratory
501 Campbell Hall #3411, University of California, Berkeley, CA,
94720, USA

PI, NASA Nexus for Exoplanet System Science

Michael P. Oman-Reagan

Department of Anthropology, Memorial University, St. John's, NL
A1C 5S7, Canada

August 22, 2017

Abstract

We discuss how visions for the futures of humanity in space and SETI are intertwined, and are shaped by prior work in the fields and by science fiction. This appears in the language used in the fields, and in the sometimes implicit assumptions made in discussions of them. We give examples from articulations of the so-called Fermi Paradox, discussions of the settlement of the Solar System (in the near future) and the Galaxy (in the far future), and METI. We argue that science fiction, especially the campy variety, is a significant contributor to the "giggle factor" that hinders serious discussion and funding for SETI and Solar System settlement projects. We argue that humanity's long-term future in space will be shaped by our short-term visions for who goes there and how. Because of the way they entered the fields, we recommend avoiding the term "colony" and its cognates when discussing the settlement of space, as well as other terms with similar pedigrees. We offer examples of science fiction and other writing that broaden and challenge our visions of human futures in space and SETI. In an appendix, we use an analogy with

SMASH: One-Shot Model Architecture Search through HyperNetworks

Andrew Brock, Theodore Lim, & J.M. Ritchie
School of Engineering and Physical Sciences
Heriot-Watt University
Edinburgh, UK
{ajb5, t.lim, j.m.ritchie}@hw.ac.uk

Nick Weston
Renishaw plc
Research Ave, North
Edinburgh, UK
Nick.Weston@renishaw.com

Abstract

Designing architectures for deep neural networks requires expert knowledge and substantial computation time. We propose a technique to accelerate architecture selection by learning an auxiliary HyperNet that generates the weights of a main model conditioned on that model's architecture. By comparing the relative validation performance of networks with HyperNet-generated weights, we can effectively search over a wide range of architectures at the cost of a single training run. To facilitate this search, we develop a flexible mechanism based on memory read-writes that allows us to define a wide range of network connectivity patterns, with ResNet, DenseNet, and FractalNet blocks as special cases. We validate our method (SMASH) on CIFAR-10 and CIFAR-100, STL-10, ModelNet10, and Imagenet32x32, achieving competitive performance with similarly-sized hand-designed networks.

1 Introduction

The high performance of deep neural nets is tempered by the cost of extensive engineering and validation to find the best architecture for a given problem. High-level design decisions such as depth, units per layer, and layer connectivity are not always obvious, and the success of models such as Inception [39], ResNets [13], FractalNets [20] and DenseNets [15] demonstrates the benefits of intricate design patterns. Even with expert knowledge, determining which design elements to weave together requires ample experimental time.

In this work, we propose to bypass the expensive procedure of fully training candidate models by instead training an auxiliary model, a HyperNet [12], to dynamically generate the weights of a main model with variable architecture. Though these generated weights are worse than freely learned weights for a fixed architecture, we leverage the observation [21] that the relative performance of different networks early in training (i.e. some distance from the eventual optimum) often provides a meaningful indication of performance at optimality. By comparing validation performance for a set of architectures using generated weights, we can approximately rank numerous architectures at the cost of a single training run.

To facilitate this search, we develop a flexible scheme based on memory read-writes that allows us to define a diverse range of architectures, with ResNets, DenseNets, and FractalNets as special cases. We validate our one-Shot Model Architecture Search through Hypernetworks (SMASH) for Convolutional Neural Networks (CNN) on CIFAR-10 and CIFAR-100 [19], Imagenet32x32 [7], ModelNet10 [41], and STL-10 [8], achieving competitive performance with similarly-sized hand-designed networks.

Opto-magnetic imaging of neural network activity in brain slices at high resolution using color centers in diamond

Mürsel Karadas[1], Adam M. Wojciechowski[2], Alexander Huck[2], Nils Ole Dalby[2,3], Ulrik Lund Andersen[2], Axel Thielscher[1,4]

Institutions:

[1]Department of Electrical Engineering, Technical University of Denmark, 2800 Kongens Lyngby, Denmark

[2]Department of Physics, Technical University of Denmark, 2800 Kongens Lyngby, Denmark

[3]Department of Drug Design and Pharmacology, Copenhagen University, 2100 Copenhagen, Denmark

[4]Danish Research Center for Magnetic Resonance, Copenhagen University Hospital, 2650 Hvidovre, Denmark

Correspondence by:

Dr. Axel Thielscher
Danish Research Center for Magnetic Resonance
Copenhagen University Hospital Hvidovre
2650 Hvidovre, Denmark
Email: axelt@drcmr.dk
Phone #: 0045-38623326

HUMAN EXPERTS VS. MACHINES IN TAXA RECOGNITION

J. Ärje[a], V. Tirronen[b], S. Kärkkäinen[a], K. Meissner[c], J. Raitoharju[d], M. Gabbouj[d], S. Kiranyaz[e]

[a] University of Jyväskylä, Department of Mathematics and Statistics, johanna.arje@jyu.fi
[b] University of Jyväskylä, Department of Information Technology
[c] Finnish Environment Institute
[d] Tampere University of Technology
[e] Qatar University

ABSTRACT

Biomonitoring of waterbodies is vital as the number of anthropogenic stressors on aquatic ecosystems keeps growing. However, the continuous decrease in funding makes it impossible to meet monitoring goals or sustain traditional manual sample processing. In this paper, we review what kind of statistical tools can be used to enhance the cost efficiency of biomonitoring: We explore automated identification of freshwater macroinvertebrates which are used as one indicator group in biomonitoring of aquatic ecosystems. We present the first classification results of a new imaging system producing multiple images per specimen. Moreover, these results are compared with the results of human experts. On a data set of 29 taxonomical groups, automated classification produces a higher average accuracy than human experts.

1. INTRODUCTION

Benthic macroinvertebrates are a diverse group of species that quickly react to changes in their environment (Rosenberg and Resh, 1993). Their community composition can reflect even subtle human-induced changes in their environment, making them an ideal indicator group for aquatic biomonitoring (Wright et al., 1984; Karr and Chu, 2000). In many countries, biomonitoring of benthic macroinvertebrates is a key part of ecological status assessment of surface waters required by the European Union's Water Framework Directive (WFD, 2000).

The traditional process of macroinvertebrate biomonitoring is presented in Fig. 1. First, macroinvertebrates are sampled, usually by using a kick-net method (e.g. Brua et al., 2011). Second, the specimen are sorted out from the detritus and identified manually by an expert. Third, the observed taxa abundancies are used to calculate several biological indices indicating changes compared to previous sampling or a reference community. Finally, the index values are combined to evaluate the ecological status of the sampled waterbody.

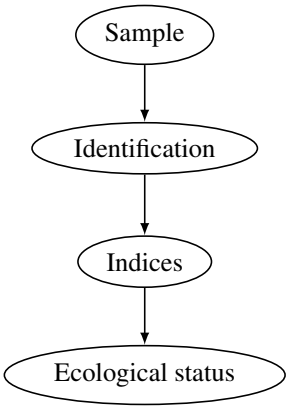

Fig. 1. The process of biomonitoring

In macroinvertebrate biomonitoring a large proportion of the total cost and time is spent on manual identification by highly trained experts. It takes several years to train an expert and manually identifying a sample of few thousand individuals can take hours. The monitoring process could be expedited substantially by shifting from manual to automated identification and in recent years there have been many studies on the automated identification of benthic macroinvertebrates (Tirronen et al., 2009; Lytle et al., 2010; Kiranyaz et al., 2010a,b; Ärje et al., 2010; Kiranyaz et al., 2011; Joutsijoki and Juhola, 2012; Joutsijoki et al., 2014; Ärje et al., 2013, 2017). Many biologists tend to oppose the shift to automated identification of macroinvertebrates due to fear of it not being accurate enough. However, manual identification has been found to be surprisingly error prone as well (Haase et al., 2010). While there exist studies on the automated classification of macroinvertebrates, to our knowledge, none of them include a comparison between manual and automated identification accuracy.

In this article we gather classification results achieved in previous studies on automated identification of macroinvertebrates on single image data. We introduce a new imaging

A Deep Structured Learning Approach Towards Automating Connectome Reconstruction from 3D Electron Micrographs

Jan Funke*, Fabian David Tschopp*, William Grisaitis, Arlo Sheridan,
Chandan Singh, Stephan Saalfeld, Srinivas C. Turaga

Abstract—We present a deep structured learning method for neuron segmentation from 3D electron microscopy (EM) which improves significantly upon the state of the art in terms of accuracy and scalability. Our method consists of a 3D U-NET architecture, trained to predict affinity graphs on voxels, followed by a simple and efficient iterative region agglomeration. We train the U-NET using a new structured loss function based on MALIS that encourages topological correctness. Our MALIS extension consists of two parts: First, we present an $O(n \log(n))$ method to compute the loss gradient, which improves over the originally proposed $O(n^2)$ algorithm. Second, we compute the gradient in two separate passes to avoid spurious gradient contributions in early training stages. Our affinity predictions are accurate enough that simple learning-free percentile-based agglomeration outperforms more involved methods used earlier on inferior predictions. We present results on three EM datasets (CREMI, FIB-25, and SEGEM) of different imaging techniques and animals where we achieve relative improvements over previous results of 27%, 15%, and 250%, respectively. Our findings suggest that a single 3D segmentation strategy can be applied to both nearly isotropic block-face EM data and anisotropic serial sectioned EM data. The runtime of our method scales with $O(n)$ in the size of the volume and achieves a throughput of about 2.6 seconds per megavoxel, qualifying our method for the processing of very large datasets.

1 INTRODUCTION

Precise reconstruction of neural connectivity is of great importance to understand the function of biological nervous systems. 3D electron microscopy (EM) is the only available imaging method with the resolution necessary to visualize and reconstruct dense neural morphology without ambiguity. At this resolution, however, even moderately small neural circuits yield image volumes that are too large for manual reconstruction. Therefore, automated methods for neuron tracing are needed to aid human analysis.

We present a structured deep learning based image segmentation method for reconstructing neurons from 3D electron microscopy which improves significantly upon state of the art in terms of accuracy and scalability. For an overview, see Fig. 1, top row. The main components of our method are: (1) Prediction of 3D affinity graphs using a 3D U-NET architecture [1], (2) a structured loss based on MALIS [2] to train the U-NET to minimize topological errors, and (3) an efficient $O(n)$ agglomeration scheme based on quantiles of predicted affinities.

The choice of using a 3D U-NET architecture to predict voxel affinities is motivated by two considerations: First, U-NETs have already shown superior performance on the segmentation of 2D [3] and 3D [1] biomedical image data. One of their favourable properties is the multi-scale architecture which enables computational and statistical efficiency. Second, U-NETs efficiently predict large regions. This is of particular interest in combination with training on the MALIS structured loss, for which we need affinity predictions in a region.

We train our 3D U-NET to predict affinities using an extension of the MALIS loss function [2]. Like the original MALIS loss, we minimize a topological error on hypothetical thresholding and connected component analysis on the predicted affinities. We extended the original formulation to derive the gradient with respect to all predicted affinities (as opposed to sparsely sampling them), leading to denser and faster gradient computation. Furthermore, we compute the MALIS loss in two passes: In the *positive pass*, we constrain all predicted affinities between and outside of ground-truth regions to be 0, and in the *negative pass*, we constrain affinities inside regions to be 1 which avoids spurious gradients in early training stages.

Although the training is performed assuming subsequent thresholding, we found iterative agglomeration of *fragments* (or "supervoxels") to be more robust to small errors in the affinity predictions. To this end, we extract fragments running a watershed algorithm on the predicted affinities. The fragments are then represented in a region adjacency graph (RAG), where edges are scored to reflect the predicted affinities between adjacent fragments: edges with small scores will be merged before edges with high scores. We discretize edge scores into k evenly distributed bins, which allows us to use a bucket priority queue for sorting. This way, the agglomeration can be carried out with a worst-case linear runtime.

The resulting method (prediction of affinities, watershed, and agglomeration) scales favourably with $O(n)$ in the size n of the volume, a crucial property for neuron segmentation from EM volumes, where volumes easily reach several

* *these authors contributed equally*